Tectonophysics, 222 (1993) 195–226
Elsevier Science Publishers B.V., Amsterdam

Petrofabric, P-wave anisotropy and seismic reflectivity of high-grade tectonites

Shaocheng Ji [a], Matthew H. Salisbury [b] and Simon Hanmer [c]

[a] *Département de Géologie, Université de Montréal, C.P. 6128, Succursale "A", Montréal, Qué. H3C 3J7, Canada*
[b] *Atlantic Geoscience Centre, Geological Survey of Canada, Bedford Institute of Oceanography, Dartmouth, N.S. B2Y 4A2, Canada*
[c] *Continental Geosciences Division, Geological Survey of Canada, 601 Booth Street, Ottawa, Ont. K1A OE4, Canada*

(Received October 28, 1992; revised version accepted January 22, 1993)

ABSTRACT

Ji, S., Salisbury, M.H. and Hanmer, S., 1993. Petrofabric, P-wave anisotropy and seismic reflectivity of high-grade tectonites. *Tectonophysics*, 222: 195–226.

In order to understand seismic anisotropy and its influence on the reflectivity of lower crustal fault zones, we have undertaken experimental measurements of P-wave velocities up to 600 MPa for 20 granulite and upper amphibolite facies mylonites from the Snowbird tectonic zone (Canada). The rocks, whose composition ranges from ultramafic to felsic, have experienced extremely large ductile strain. It is found that the amphibolitic mylonites exhibit significant V_p anisotropy (6–13% at 600 MPa), whereas the pyroxene-bearing granulite-facies mylonites and the quartz or feldspathic (tonalitic, granitic and diatexitic) mylonites are quasi-isotropic. In order to constrain interpretation of the measured V_p properties, microstructural analyses have been systematically performed in the samples studied. It is shown that the interaction between feldspar and quartz or pyroxene and the absence of amphibole cause anisotropy in the granulite facies mylonites to be low. The amphibolitic mylonites are strongly anisotropic because of a large volume fraction of hornblende with strong LPO ([001]‖lineation, and (100)‖foliation). The anisotropy pattern in the amphibolitic mylonites is consistently orthorhombic: $V_p(X) > V_p(Y) > V_p(Z)$, where X is parallel to stretching lineation, Y is normal to the lineation in the foliation plane and Z is normal to the foliation plane. But the anisotropy pattern in the mica-rich mylonites is transversely isotropic: $V_p(X) = V_p(Y) > V_p(Z)$. If sufficiently large volumes of the crust display such patterns, this difference may be an important indicator for kinematic analysis in the middle to lower crust using modern seismic techniques. The study demonstrates that while seismic reflectivity is strongly lithology-controlled, fabric-induced anisotropy can both enhance and decrease seismic reflectivity. Hence, the discontinuity of seismic reflections along ductile shear zones in the lower crust is not necessarily indicative of the discontinuity of the shear zones, but may indicate changes in composition or metamorphic grade.

1. Introduction

Seismic reflectivity in the deep continental crust is generally attributed to impedance contrasts associated with compositional layering and lithological heterogeneity (e.g., Meissner, 1973; McDonough and Fountain, 1988), to impedance contrasts caused by fluids trapped in microcracks and pores (Jones and Nur, 1984) and to interference effects. It has also been proposed that crustal reflections can be caused by fabric-related velocity anisotropy in ductile shear zones (e.g., Etheridge and Vernon, 1983; Fountain et al., 1984). Many greenschist and lower amphibolite facies shear zones in the middle crust, for example, the Lewisian mylonite zone in Scotland (Fountain et al., 1984), the Brevard mylonite zone (Christensen and Szymanski, 1988), the Santa Rosa mylonite zone in California (Kern and Wenk, 1990),

Correspondence to: Shaocheng Ji, Département de Géologie, Université de Montréal, C.P. 6128, Succursale "A", Montréal, Qué. H3C 3J7, Canada

and the Whipple Mountain detachment fault (Wang et al., 1989), have been shown to be good reflectors due to seismic anisotropy induced by extensive lattice preferred orientation (LPO) of phyllosilicate minerals such as biotite and muscovite in the plane of foliation. Although many investigators have interpreted mid-crustal reflectors in term of fault zones (e.g., Barazangi and Brown, 1986; Leven et al., 1990; Meissner et al., 1991), conditions in the lower crust are quite different and the association is less clear: (a) upper amphibolite and granulite facies metamorphic rocks predominate ($T > 700°C$) and phyllosilicate minerals are volumetrically insignificant; and (b) the confining pressure (600–1000 MPa) is high enough to close all microcracks. In order to interpret deep continental seismic reflection data, it is necessary to evaluate the reflectivity of high-grade ductile shear zones. To this end, we have experimentally investigated the compressional wave velocity and anisotropy of very strongly deformed rocks (mylonites and ultramylonites) from the upper amphibolite and granulite facies terrane of the Snowbird tectonic zone in northern Saskatchewan, Canada. Particular attention has been paid to determining the origin and possible kinematic implications of lower crustal anisotropy.

2. Samples and their geological setting

The rock samples studied were collected from the Tantato high-grade metamorphic domain in northern Saskatchewan (Fig. 1). This domain consists of a large (75×120 km), highly strained triangular fault block in the Snowbird tectonic zone containing two structural decks (Hanmer et al., 1991). The fan-shaped lower deck is characterised by granulite and upper amphibolite facies mylonites with steep foliations and a shallow to moderate SW-plunging extension lineation. The arcuate upper deck is characterised by mafic granulite and diatexite with shallow, southwest-dipping foliations parallel to its NW–SE-trending margin. All stretching lineations in the upper deck display a shallow plunge toward the southwest. Dextral and sinistral shear occurred 2.6–3.2 Ga along the western and eastern parts, respectively, of the lower deck (R. Parrish, pers. commun., 1991). The upper deck seems to have been initially emplaced by thrusting, although abundant structural evidence shows subsequent low-angle, ductile normal faulting (post-granulite facies) in the hornblende granite (Mary batholith) boundary mylonite between the hanging wall and footwall (Fig. 1a). More than 400 oriented samples were collected from the Tantato high-grade mylonite terrane, of which 20 representative samples ranging from ultramafic through acidic in composition were selected for the present study (Fig. 1b). Foliation and lineation can be clearly identified in all samples, allowing the specimens to be oriented with respect to an orthogonal reference system in which X lies parallel to the stretching lineation, Y is normal to the lineation in the foliation plane, and Z is normal to the foliation plane.

Modal analyses of the samples are given in Table 1. The modal content of each sample was determined by point counting, with 1500 points being counted for each sample. The geological context and microstructural features of each sample are summarized below:

2.1 Ultramafic mylonites

J152 is a mylonitic pyroxenite with a medium grain size (0.05–0.10 mm). Orthopyroxene (ferrosilite) forms prismatic plates with aspect ratios ranging from 4 : 1 to 12 : 1, and contains numerous homogeneous kink-bands whose kink-band boundaries (KBB) are subperpendicular to the foliation and lineation. Intracrystalline strain in the clinopyroxene (diopside) is characterized by undulose to patchy extinction and the development of subgrains (Fig. 2a). The opx-cpx geothermometer (Wells, 1977) gives a temperature of around 860°C, corresponding to the last equilibration of the two pyroxenes. Xenomorphic amphibole (magnesio-hornblende) grains formed during retrograde metamorphism from the granulite to the amphibolite facies are isolated in a matrix of ortho- and clino-pyroxene grains (Fig. 2a).

J311 is a mylonitic magnesio-hornblendite collected from a large inclusion in diatexitic mylonite. The latter deformed at about 650°C and

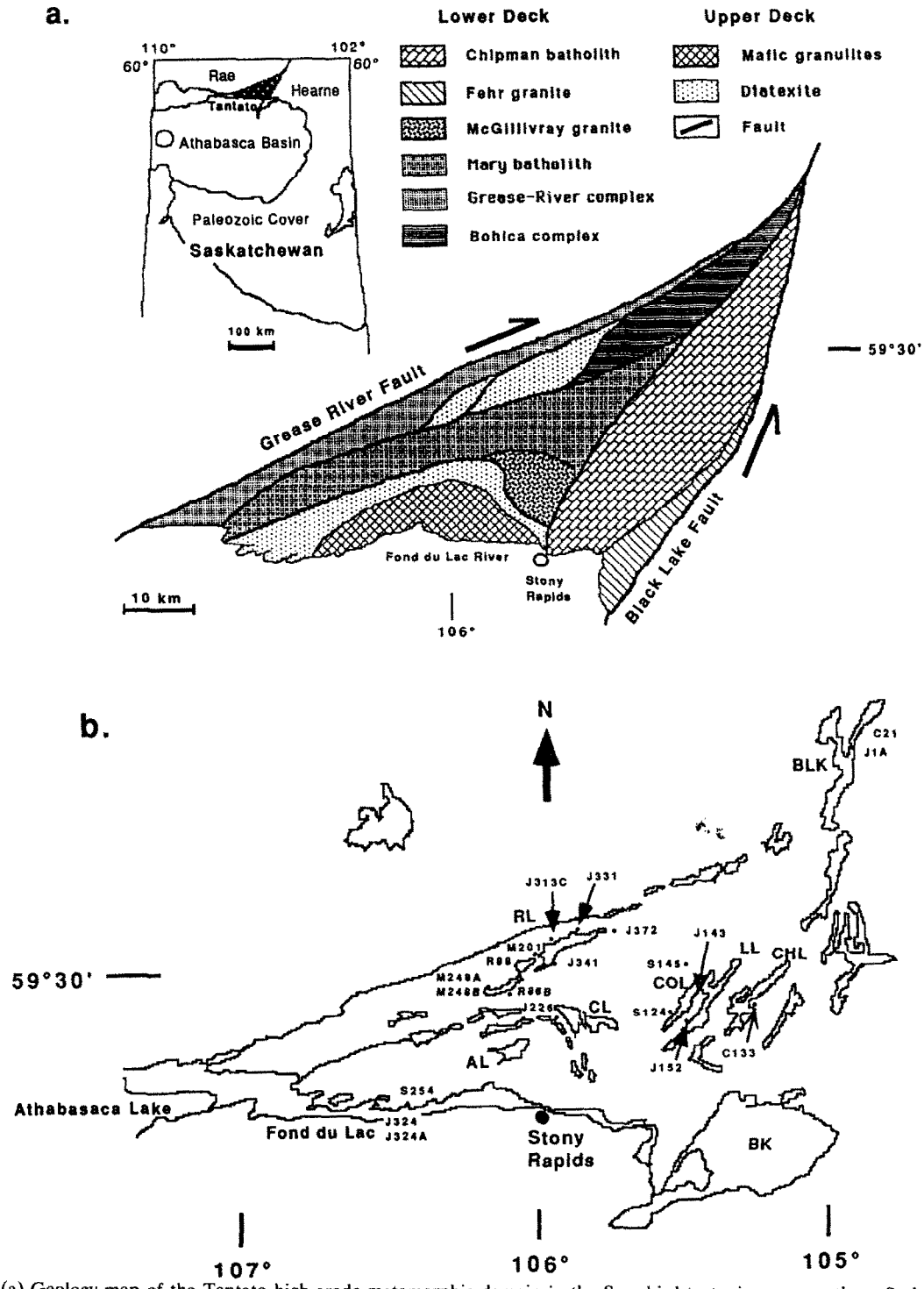

Fig. 1. (a) Geology map of the Tantato high-grade metamorphic domain in the Snowbird tectonic zone, northern Saskatchewan, Canada (insert). (b) Locations of samples used in present study. The Chipman batholith consists of annealed tonalitic straight gneisses, clinopyroxene-bearing tonalite ribbon mylonites, deformed or undeformed mafic dykes and dispersed pyroxenite inclusions. The Mary batholith is characterized by compositionally monotonous, garnet-hornblende granitic to granodioritic mylonites. The Grease-River complex consists of granitic and diatexitic mylonites and ultramylonites with dispersed inclusions of pyroxenite and hornblendite. The Bohica complex consists of strongly deformed anorthosite, norite, gabbro and diorite. The Fehr granite and McGillivray granite are generally isotropic and extremely coarse grained. *AL* = Axis lake; *BK* = Black lake; *BLK* = Bompas lake; *CHL* = Chipman lake; *CL* = Clut lake; *COL* = Cora lake; *LL* = Lytle lake; and *RL* = Reeve lake.

650 MPa, based on estimates using the garnet/hornblende geothermometer of Graham and Powell (1984) and the hornblende geobarometer of Hollister et al. (1987). The sample displays a recrystallization-induced bimodal grain size distribution (Fig. 2b). Serpentinization took place along late brittle microfractures and produced Fe-oxides.

2.2 *Mafic mylonites*

Samples C21 and J1A are fine grained (50–150 μm), amphibolitic ultramylonites formed under amphibolite facies conditions from a mafic dyke in the Chipman batholith. Well-developed compositional banding is defined by alternating layers consisting predominantly of magnesio-hornblende and plagioclase (An35–50). Lath-shaped hornblende and equant plagioclase microstructures suggest that the rock has been completely recrystallized (Fig. 2c). Most of the subhedral hornblende grains show no evidence of internal deformation although some grains display undulose extinction and subgrains. The geobarometer of Hammarstrom and Zen (1986) gives a pressure of about 430 MPa.

R86B, J313C, J341 and J143 are amphibolitic mylonites in which magnesio-hornblende appears as both porphyroclasts and recrystallized fine grained matrix, whereas plagioclase is completely

TABLE 1

Modal analyses (vol.%) of samples from the Snowbird Tectonic Zone

Sample no.	Rock type	Modal analysis											
		bi	cpx	gt	hb	kf	op	opx	pl	qtz	ser	chl	others
Ultramafic													
J152	mylonitic pyroxenite	–	39.0	–	28.9	–	1.2	28.6	–	–	–	–	2.3 tal
J311	hornblenditic mylonite	–	–	–	60.2 *	–	5.4	–	–	–	–	–	2.5 ol, 23.3 serp, 5.3 sp, 3.3 tal
Mafic													
C21	amphibolitic ultramylonite	–	–	–	69.2	–	3.2	–	25.3	–	1.5	–	0.8 acc
J1A	amphibolitic ultramylonite	–	–	–	65.0	–	0.2	–	28.9	0.2	4.2	0.4	1.1 acc
R86B	amphibolitic mylonite	–	0.5	1.5	65.0	–	1.1	–	20.1	6.1	0.4	5.3	
J313C	amphibolitic mylonite	0.6	0.6	–	61.2	–	–	–	37.0	–	–	0.6	–
J341	amphibolitic mylonite	1.4	–	–	58.0	–	2.1	–	24.1	5.6	1.2	7.5	0.1 ca
J143	cpx-gt mylonitic amphibolite	–	11.7	4.1	61.8	–	1.2	–	19.2	–	0.8	0.7	0.4 clz, 0.1 mus
J324	mafic ultramylonite	1.1	12.6	–	0.4	–	1.0	10.3	66.2	–	7.4	1.0	–
J324A	mafic ultramylonite	1.6	18.2	–	12.0	–	0.8	10.8	55.2	–	1.4	–	
S254	mafic ultramylonite	–	11.4	–	8.5	–	4.0	5.1	69.7	–	0.4	0.4	0.4 nd, 0.1 zir
Intermediate													
S145	protomylonitic anorthosite	–	–	–	–	–	1.0	–	83.2	5.1	10.0	0.1	0.6 nd
S124	gt-hb tonalitic ultramylonite	1.0	–	4.3	7.2	–	0.4	–	59.7	26.0	–	–	1.4 ca
C133	annealed tonalitic mylonite	4.6	–	0.1	8.6	–	–	–	54.0	32.5	–	0.1	0.1 zir
Acidic													
J372	hb-gt granitic mylonite	8.1	–	5.4	16.8	25.1	0.8	–	12.8	30.0	0.6	–	0.4 zir
J226	hb-granitic "s-c" mylonite	8.6	–	0.5	23.5	29.1	1.2	–	13.7	22.9	0.1	–	0.4 ca
M201	diatexitic ultramylonite	–	–	2.0	–	51.5	0.4	–	–	46.1	–	–	–
R88	diatexitic ultramylonite	2.9	–	2.3	–	45.5	0.5	–	–	48.8	–	–	–
M248B	granitic mylonite	3.4	–	1.2	–	65.0	–	–	1.4	29.0	–	–	–
M248A	gt-bi granitic ultramylonite	34.2	–	6.8	–	14.4	0.8	–	12.6	29.9	0.9	–	0.4 zir

Abbreviations: acc = accessories, bi = biotite, ca = calcite, chl = chlorite, clz = clinozoisite, cpx = clinopyroxene, gt = garnet, hb = hornblende, hb * = tremolite, kf = K-feldspar, mus = muscovite, nd = undetermined minerals, ol = olivine, op = opaque minerals, opx = orthopyroxene, pl = plagioclase, qtz = quartz, ser = sericite, serp = serpentine, sp = spinel, tal = talc, zir = zircon.

recrystallized (Fig. 2d). The hornblende-garnet geobarometer (Hollister et al., 1987) and clinopyroxene-garnet geothermometer (Ellis and Green, 1979) show that deformation took place at approximately 700 MPa and 700°C.

Samples J324, J324A and S254 are the typical mafic granulite (pyriclasite) mylonites in the hanging wall (Fig. 1). They consist of plagioclase (An50–65), clinopyroxene (diopside-augite), orthopyroxene (hypersthene), and opaque minerals.

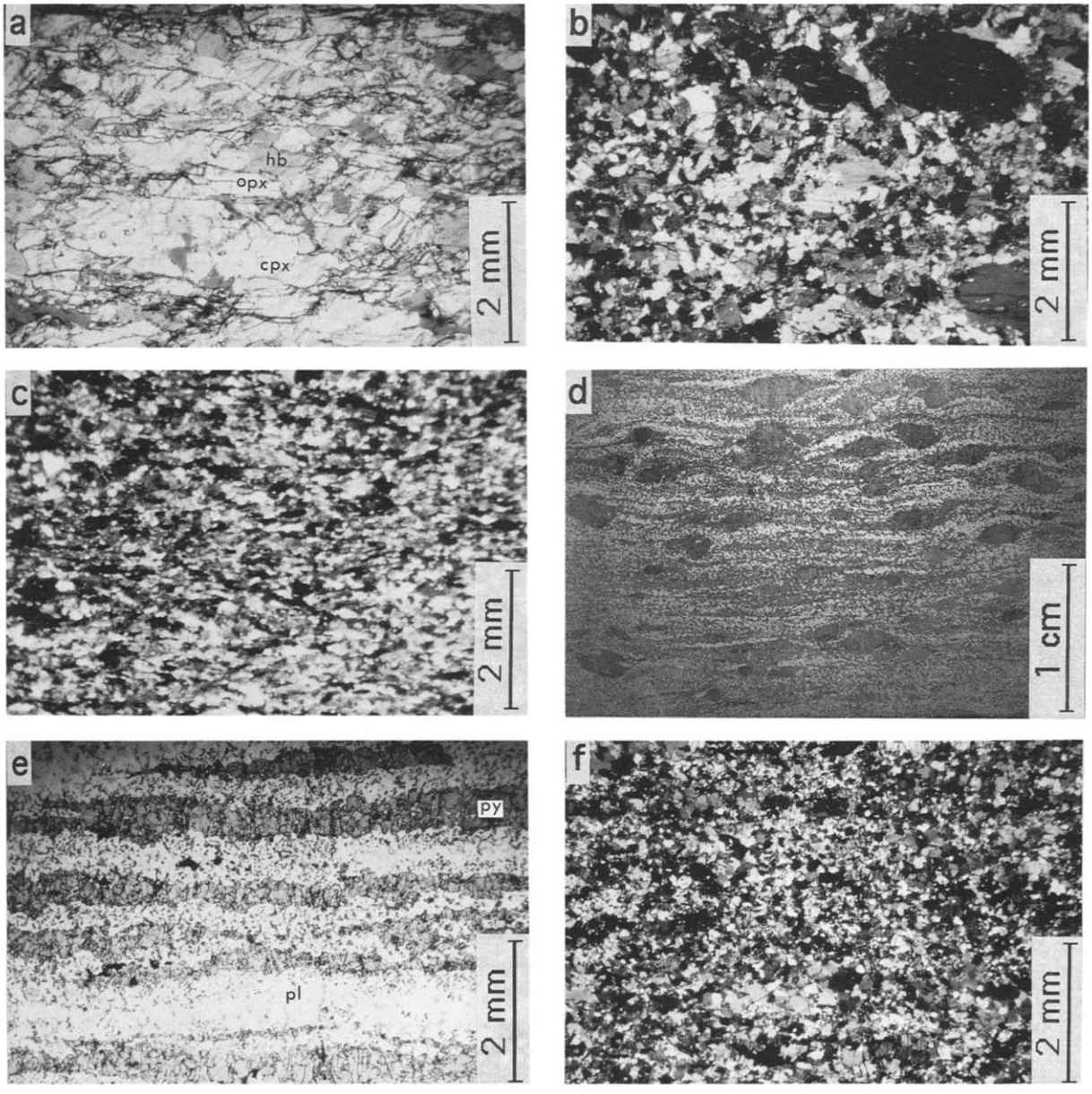

Fig. 2. Microstructural features of samples from the Tantato domain. (a) Deformed pyroxenite (J152). Hornbende nucleated and grew at the expense of orthopyroxene and clinopyroxene. (b) Recrystallization-induced bimodal grain-size distribution in hornblendite (J311). (c) Ultramylonitic microstructure in amphibolite (J1A). (d) Amphibolitic mylonite (J313C) showing hornblende porphyroclasts in a matrix of plagioclase and recrystallized hornblende. (e) and (f) Mafic granulite (pyriclasite) ultramylonite (J324). The microstructure is characterized by elongate polycrystalline ribbons of recrystallized pyroxene in a completely recrystallized matrix of plagioclase.

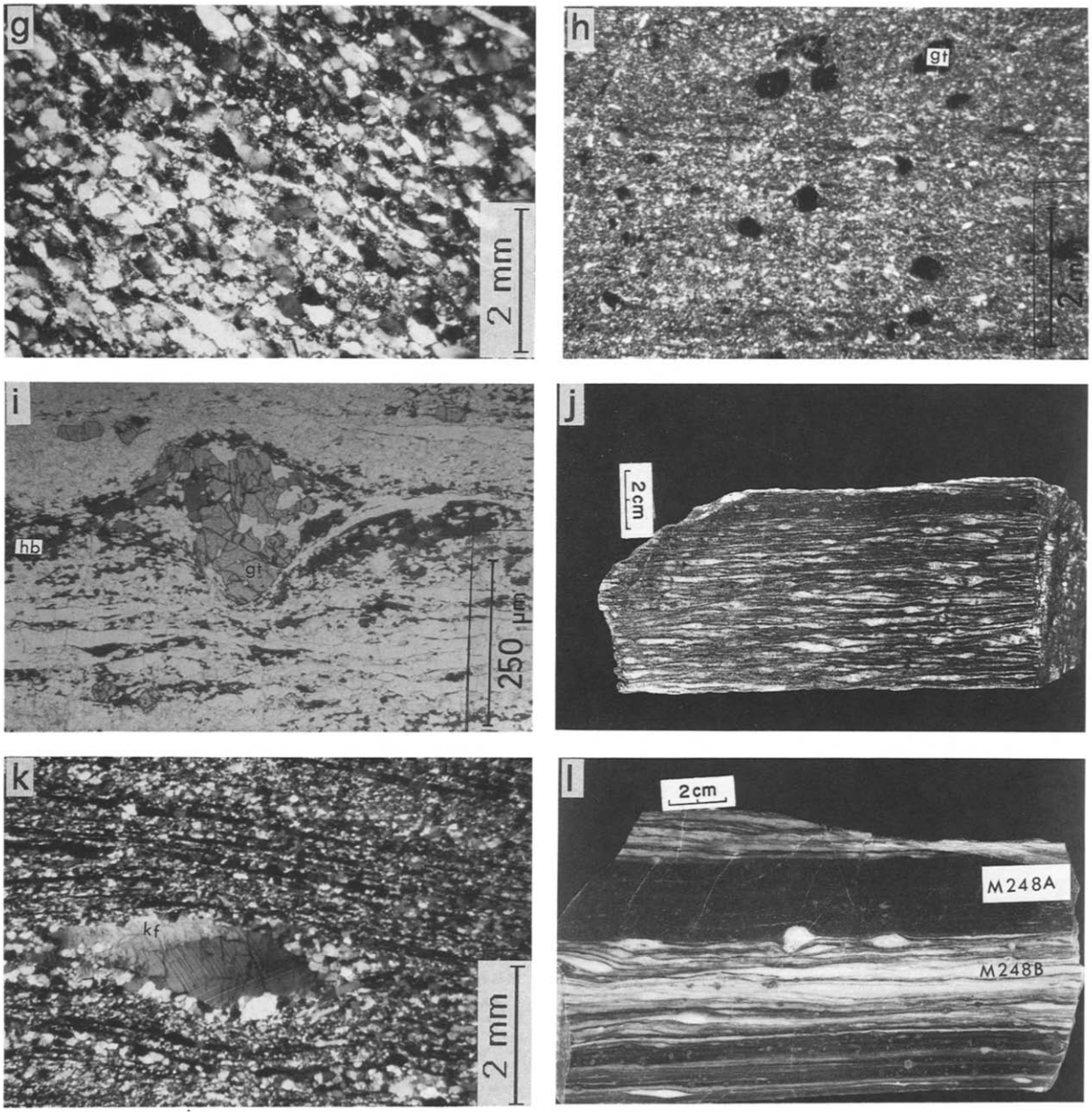

Fig. 2. (g) Foliated and lineated protomylonitic anorthosite (S145). Intracrystalline deformation features such as tapered or bent mechanical twins, undulatory extinction, and recrystallization are abundant. (h) Ultramylonitic microstructure in sample S124. Porphyroclasts/porphyroblasts of garnet are dispersed in a fine-grained, recrystallized quartz-plagioclase matrix. (i) Hornblende and garnet-bearing granitic mylonite (J372). Note garnet porpyroclasts with attenuated polycrystalline tails of hornblende which nucleated and grew at the expense of garnet during synkinematic retrograde metamorphism. (j) Extensional shear bands in hornblende-granitic mylonite (J226). (k) Recrystallized K-feldspar porphyroclast in strongly deformed quartzofeldspathic matrix in diatexitic ultramylonite (M201). (l) Diatexitic ultramylonite and mylonite. M248A is cored from the biotite-rich layer (dark) and M248B from the quartzofeldspathic layer (light). Quartz forms hair-like ribbons and K-feldspar is recrystallized to form polycrystalline streaks.

J324A and S254 contain about 10% hornblende, indicating some degree of retrograde metamorphism. The foliation is parallel to metamorphic banding defined by alternating plagioclase- and pyroxene-rich layers (0.02–1.00 cm thick). The lineation is well defined by elongate polycrys-

talline ribbons of recrystallized orthopyroxene and clinopyroxene (Fig. 2e and f). The deformation temperature is estimated from the two pyroxene thermometer of Wells (1977) to have been 830°C, which agrees with the results (870°C, 860 MPa) determined from associated rocks containing garnet-orthopyroxene/clinopyroxene-plagioclase-quartz (temperature from Moecher et al., 1988; pressure from Perkins and Newton, 1981).

2.3 Intermediate mylonites

S145 is a foliated and lineated protomylonitic anorthosite. The plagioclase (An50–70) with an average grain-size of 0.4 mm displays optical evidence of plastic deformation (Fig. 2g), such as undulatory extinction, curved tapering deformation twins, kink bands, subgrains and very small recrystallized new grains (30–50 μm). The anorthosite does not permit estimation of the temperature and pressure conditions of deformation or metamorphism. However, the Hodges and Spear (1982) geothermometer and the Newton and Haselton (1981) geobarometer give a temperature of 720–740°C and a pressure of about 500 MPa for the surrounding country rocks (diatexite containing gt-pl-bi-sil-qtz).

C133 is a typical medium-grained (0.3–1.0 mm), annealed tonalitic mylonite from the Chipman batholith. The sample displays plagioclase- and quartz-rich straight layers with a sugary texture and strong lineation defined by elongate hornblende. The Hodges and Spear (1982) geothermometer gives a temperature of about 700°C. S124 is a splendid, very fine-grained ultramylonite (< 25 μm) with a tonalitic composition (Fig. 2h).

2.4 Acidic mylonites

J372 and J226 are fine to medium-grained hornblende-bearing granitic mylonites. Quartz occurs as polycrystalline or monocrystalline ribbons and feldspar as recrystallized grains. In J372, garnet porphyroclasts have attenuated polycrystalline tails of hornblende (ferro-edenite), which nucleated and grew at the expense of garnet during retrogression from granulite to amphibolite facies (Fig. 2i). The temperature and pressure of synkinematic metamorphism are estimated from the garnet-hornblende thermometer (Graham and Powell, 1984) to be 650°C and 650 MPa. J226 displays typical extensional shear bands (Fig. 2j) with hornblende and biotite aligned parallel to both the foliation and shear planes.

Samples M201, R88 and M248B are fine-grained (30–60 μm), granulite facies diatexitic ultramylonites and mylonites. Quartz displays an elongate hair-like ribbon structure, whereas K-feldspar is almost completely recrystallized into fine grained neoblasts, forming polycrystalline streaks (Fig. 2k, l). Isolated coarse porphyroclasts of K-feldspar (1–5 cm) are occasionally observed in outcrop, indicating that strong deformation and grain size reduction have taken place. The gt-pl-bi-sil-qtz geothermobarometer (Newton and Haselton, 1981) gives a temperature of 700°C and a pressure of around 700 MPa. M248A was cut from a narrow, very fine-grained ultramylonite layer in sample M248B (Fig. 2l). Compared with its surrounding rock (M248B), M248A is obviously rich in biotite and garnet, implying that it experienced significant retrograde metamorphism during ultramylonitization.

3. Velocity measurements

3.1 Experimental method

Three cores (2.54 cm in diameter and 5–7 cm in length) were cut from each sample in the X, Y and Z directions, respectively. These cores were then jacketed in thin copper foil and gum rubber tubing to prevent the pressure medium from penetrating the sample at high pressure. The samples were then placed in a large-volume (3.3 l) pressure vessel and compressional wave velocity measurements carried out at various hydrostatic confining pressures up to 600 MPa using the pulse transmission technique (Birch, 1960). The pressure was controlled by an air-driven fluid pump and a hydraulic intensifier, and determined to within 0.1 MPa by direct digital readout from a calibrated strain guage. The ultrasonic waves were generated and received by 1-MHz lead zirconate piezoelectric transducers mounted on each end of

TABLE 2

Compressional wave velocities at various confining pressures for high-grade mylonites in the Snowbird Tectonic Zone

Average density (g/cm^3)	Propagation direction	Pressure (MPa)												Pressure derivatives		
		10	20	40	60	80	100	150	200	300	400	500	600	$(V_p)_0$	(dV_p/dP) $\times 10^4$	R^2
J152 mylonitic pyroxenite																
3.29	*X*	7.70	7.75	7.82	7.86	7.89	7.91	7.93	7.95	7.97	7.99	8.00	8.02	7.918	1.70	0.99
	Y	7.36	7.40	7.46	7.50	7.52	7.53	7.56	7.58	7.60	7.61	7.63	7.65	7.546	1.70	0.99
	Z	7.38	7.43	7.52	7.57	7.59	7.61	7.63	7.64	7.65	7.67	7.68	7.70	7.608	1.50	0.99
	mean V_p	7.48	7.53	7.60	7.64	7.67	7.68	7.71	7.72	7.74	7.76	7.77	7.79	7.688	1.70	0.99
	A%	4.6	4.7	4.7	4.7	4.8	5.0	4.8	4.8	4.8	4.9	4.8	4.8			
J311 hornblenditic mylonite																
3.08	*X*	7.07	7.10	7.16	7.19	7.21	7.23	7.26	7.28	7.31	7.34	7.36	7.39	7.233	2.60	0.99
	Y	6.84	6.89	6.96	6.98	7.00	7.02	7.03	7.05	7.06	7.08	7.10	7.12	7.000	2.00	1.00
	Z	6.38	6.43	6.49	6.52	6.54	6.56	6.58	6.60	6.62	6.64	6.66	6.68	6.560	2.00	1.00
	mean V_p	6.76	6.81	6.87	6.90	6.92	6.94	6.96	6.98	7.00	7.02	7.04	7.06	6.940	2.00	1.00
	A%	10.2	9.8	9.8	9.7	9.7	9.7	9.8	9.7	9.9	10.0	9.9	10.1			
C21 amphibolitic ultramylonite																
3.02	*X*	7.28	7.31	7.34	7.35	7.36	7.37	7.39	7.41	7.42	7.43	7.45	7.46	7.377	1.40	0.98
	Y	6.75	6.79	6.82	6.84	6.86	6.87	6.89	6.90	6.92	6.93	6.94	6.95	6.890	1.00	1.00
	Z	6.44	6.50	6.57	6.60	6.62	6.63	6.66	6.67	6.68	6.69	6.70	6.71	6.650	1.00	1.00
	mean V_p	6.82	6.87	6.91	6.93	6.95	6.96	6.98	6.99	7.01	7.02	7.03	7.04	6.980	1.00	1.00
	A%	12.3	11.8	11.1	10.8	10.7	10.6	10.5	10.6	10.6	10.5	10.7	10.7			
J1A amphibolitic ultramylonite																
3.00	*X*	7.10	7.22	7.28	7.32	7.33	7.34	7.36	7.37	7.38	7.39	7.39	7.40	7.363	0.60	0.90
	Y	6.67	6.77	6.85	6.90	6.92	6.95	6.98	7.01	7.03	7.05	7.06	7.07	6.994	1.30	0.97
	Z	6.18	6.27	6.35	6.40	6.43	6.47	6.52	6.55	6.58	6.60	6.62	6.63	6.531	1.70	0.98
	mean V_p	6.65	6.75	6.83	6.87	6.89	6.92	6.95	6.98	7.00	7.01	7.02	7.03	6.970	1.00	1.00
	A%	13.8	14.1	13.6	13.4	13.1	12.6	12.1	11.8	11.4	11.3	11.0	11.0			
R86B amphibolitic mylonite																
3.01	*X*	6.86	6.97	7.08	7.15	7.19	7.22	7.26	7.28	7.30	7.31	7.32	7.33	7.270	1.00	1.00
	Y	6.38	6.50	6.74	6.85	6.92	6.98	7.04	7.08	7.10	7.11	7.12	7.13	7.070	1.00	1.00
	Z	–	–	–	–	–	6.46	6.54	6.57	6.61	6.62	6.64	6.66	6.556	1.70	0.98
	mean V_p	–	–	–	–	–	6.89	6.95	6.98	7.00	7.01	7.03	7.04	6.957	1.40	0.98
	A%	–	–	–	–	–	11.0	10.4	10.2	9.9	9.8	9.7	9.5			
J313C amphibolitic mylonite																
2.97	*X*	6.91	7.16	7.32	7.39	7.43	7.45	7.48	7.50	7.52	7.54	7.55	7.57	7.473	1.60	0.99
	Y	6.54	6.75	6.89	6.95	6.98	7.00	7.02	7.04	7.06	7.08	7.00	7.12	7.000	2.00	1.00
	Z	5.78	6.00	6.32	6.40	6.46	6.49	6.53	6.56	6.59	6.61	6.64	6.66	6.517	2.40	0.99
	mean V_p	6.41	6.64	6.84	6.91	6.96	6.98	7.01	7.03	7.06	7.08	7.06	7.12	7.000	2.00	1.00
	A%	17.6	17.5	14.6	14.3	13.9	13.8	13.6	13.4	13.2	13.1	12.9	12.8			
J341 amphibolitic mylonite																
2.97	*X*	7.16	7.20	7.25	7.27	7.29	7.30	7.32	7.33	7.34	7.35	7.36	7.37	7.310	1.00	1.00
	Y	6.77	6.90	6.96	7.00	7.02	7.04	7.06	7.08	7.10	7.11	7.13	7.14	7.057	1.40	0.98
	Z	6.01	6.14	6.25	6.31	6.34	6.36	6.40	6.42	6.45	6.47	6.49	6.51	6.390	2.00	1.00
	mean V_p	6.65	6.75	6.82	6.86	6.88	6.90	6.93	6.94	6.96	6.98	6.99	7.01	6.913	1.60	0.99
	A%	17.3	15.7	14.7	14.0	13.8	13.6	13.3	13.1	12.8	12.6	12.5	12.3			

TABLE 2 (continued)

Average density (g/cm^3)	Propagation direction	Pressure (MPa)												Pressure derivatives		
		10	20	40	60	80	100	150	200	300	400	500	600	$(V_p)_0$	(dV_p/dP) $\times 10^4$	R^2
J143 mylonitic amphibolite																
3.20	*X*	7.03	7.24	7.32	7.35	7.37	7.38	7.39	7.40	7.41	7.42	7.43	7.44	7.380	1.00	1.00
	Y	6.58	6.67	6.78	6.83	6.87	6.89	6.93	6.97	7.00	7.02	7.04	7.06	6.940	2.00	1.00
	Z	6.53	6.64	6.74	6.79	6.83	6.87	6.91	6.93	6.96	6.98	7.00	7.02	6.900	2.00	1.00
	mean V_p	6.71	6.85	6.95	6.99	7.02	7.05	7.08	7.10	7.12	7.14	7.16	7.17	7.071	1.70	0.98
	A%	7.5	8.8	8.4	8.0	7.7	7.2	6.8	6.6	6.3	6.2	6.0	5.9			
J324 mafic mylonite																
2.92	*X*	6.87	6.90	6.93	6.95	6.97	6.98	7.01	7.03	7.05	7.06	7.07	7.08	7.020	1.00	1.00
	Y	6.74	6.78	6.85	6.89	6.92	6.93	6.95	6.96	6.97	6.98	6.98	6.99	6.953	0.60	0.90
	Z	6.83	6.92	6.95	6.97	6.98	6.99	7.01	7.02	7.03	7.04	7.06	7.07	6.987	1.40	0.98
	mean V_p	6.81	6.87	6.91	6.94	6.96	6.97	6.99	7.00	7.02	7.03	7.04	7.05	6.990	1.00	1.00
	A%	1.9	2.0	1.5	1.2	0.9	0.9	0.9	1.0	1.1	1.1	1.3	1.3			
J324A mafic mylonite																
2.95	*X*	6.69	6.89	6.94	6.97	6.99	7.00	7.03	7.04	7.05	7.06	7.07	7.07	7.031	0.70	0.89
	Y	6.60	6.70	6.78	6.83	6.86	6.89	6.93	6.96	6.99	7.00	7.01	7.02	6.960	1.00	1.00
	Z	6.79	6.83	6.87	6.90	6.92	6.94	6.96	6.98	6.99	7.00	7.00	7.01	6.973	0.60	0.90
	mean V_p	6.69	6.81	6.86	6.90	6.92	6.94	6.97	6.99	7.01	7.02	7.03	7.03	6.991	0.70	0.89
	A%	2.8	2.8	2.3	2.0	1.9	1.6	1.4	1.1	0.9	0.9	1.0	0.9			
S254 mafic mylonite																
2.87	*X*	6.41	6.55	6.68	6.75	6.79	6.82	6.86	6.88	6.91	6.92	6.94	6.95	6.867	1.40	0.98
	Y	6.31	6.45	6.55	6.62	6.65	6.70	6.75	6.78	6.82	6.84	6.85	6.86	6.784	1.30	0.97
	Z	6.24	6.32	6.50	6.60	6.65	6.67	6.71	6.73	6.76	6.77	6.78	6.79	6.730	1.00	1.00
	mean V_p	6.32	6.44	6.58	6.66	6.70	6.73	6.77	6.77	6.83	6.84	6.86	6.87	6.787	1.40	0.98
	A%	2.7	3.6	2.7	2.3	2.1	2.2	2.2	2.2	2.2	2.2	2.3	2.3			
S145 protomylonitic anorthosite																
2.74	*X*	6.05	6.12	6.28	6.38	6.45	6.50	6.57	6.60	6.63	6.65	6.68	6.70	6.557	2.40	0.99
	Y	6.00	6.08	6.26	6.36	6.43	6.49	6.55	6.58	6.61	6.64	6.66	6.68	6.544	2.30	0.99
	Z	6.09	6.17	6.30	6.41	6.47	6.52	6.60	6.63	6.68	6.72	6.73	6.75	6.621	2.20	0.93
	mean V_p	6.05	6.12	6.28	6.38	6.45	6.50	6.57	6.60	6.64	6.67	6.69	6.71	6.574	2.30	0.99
	A%	1.5	1.5	0.6	0.8	0.6	0.5	0.8	0.8	1.1	1.2	1.1	1.0			
S124 tonalitic mylonite																
2.74	*X*	6.68	6.69	6.72	6.74	6.75	6.77	6.79	6.80	6.82	6.83	6.84	6.85	6.790	1.00	1.00
	Y	6.75	6.78	6.81	6.83	6.85	6.86	6.88	6.89	6.91	6.92	6.93	6.95	6.869	1.30	0.97
	Z	6.77	6.80	6.83	6.85	6.87	6.88	6.90	6.91	6.92	6.94	6.95	6.96	6.884	1.30	0.97
	mean V_p	6.73	6.76	6.79	6.81	6.82	6.84	6.86	6.87	6.88	6.90	6.91	6.92	6.844	1.30	0.97
	A%	1.3	1.6	1.6	1.6	1.8	1.6	1.6	1.6	1.5	1.6	1.6	1.6			
C133 annealed tonalitic mylonite																
2.68	*X*	6.10	6.17	6.32	6.38	6.42	6.45	6.49	6.51	6.53	6.55	6.56	6.58	6.483	1.60	0.99
	Y	5.93	6.05	6.11	6.13	6.15	6.16	6.19	6.20	6.23	6.26	6.29	6.32	6.140	3.00	1.00
	Z	5.94	6.06	6.12	6.14	6.17	6.18	6.21	6.24	6.26	6.29	6.32	6.35	6.170	3.00	1.00
	mean V_p	5.99	6.09	6.18	6.22	6.25	6.26	6.30	6.32	6.34	6.37	6.39	6.42	6.263	2.60	0.99
	A%	2.8	2.0	3.4	4.0	4.3	4.6	4.8	4.9	4.7	4.6	4.2	4.1			

TABLE 2 (continued)

Average density (g/cm^3)	Propagation direction	Pressure (MPa)												Pressure derivatives		
		10	20	40	60	80	100	150	200	300	400	500	600	$(V_p)_0$	(dV_p/dP) $\times 10^4$	R^2
J372 hb-gt granitic mylonite																
2.84	X	5.74	5.88	6.05	6.17	6.23	6.27	6.33	6.38	6.43	6.45	6.48	6.51	6.346	2.70	0.99
	Y	5.62	5.83	6.02	6.13	6.20	6.25	6.32	6.36	6.41	6.44	6.46	6.49	6.333	2.60	0.99
	Z	4.65	4.90	5.27	5.52	5.67	5.78	5.93	6.01	6.10	6.16	6.21	6.25	5.955	5.00	0.99
	mean V_p	5.34	5.54	5.78	5.94	6.03	6.10	6.19	6.25	6.31	6.35	6.38	6.42	6.203	3.60	1.00
	$A\%$	20.4	17.7	13.5	10.9	9.3	8.0	6.5	5.9	5.2	4.6	4.2	4.1			
J226 hb granitic mylonite																
2.76	X	5.92	6.00	6.08	6.13	6.17	6.20	6.24	6.27	6.29	6.31	6.33	6.35	6.230	2.00	1.00
	Y	5.71	5.85	5.94	5.99	6.02	6.05	6.09	6.11	6.14	6.16	6.18	6.21	6.069	2.30	0.99
	Z	5.46	5.59	5.72	5.80	5.84	5.88	5.93	5.96	5.99	6.02	6.04	6.07	5.913	2.60	0.99
	mean V_p	5.70	5.81	5.91	5.97	6.01	6.04	6.09	6.11	6.14	6.16	6.18	6.21	6.069	2.30	0.99
	$A\%$	8.1	7.1	6.1	5.5	5.5	5.3	5.1	5.1	4.9	4.7	4.7	4.5			
M201 diatexitic ultramylonite																
2.63	X	5.30	5.45	5.68	5.79	5.85	5.90	5.95	5.98	6.02	6.04	6.06	6.07	5.971	1.70	0.98
	Y	5.53	5.79	5.95	6.06	6.11	6.15	6.21	6.25	6.29	6.31	6.33	6.35	6.230	2.00	1.00
	Z	5.44	5.55	5.70	5.85	5.92	5.98	6.05	6.10	6.14	6.16	6.17	6.18	6.104	1.30	0.97
	mean V_p	5.42	5.57	5.78	5.90	5.96	6.01	6.07	6.11	6.15	6.17	6.19	6.20	6.101	1.70	0.98
	$A\%$	4.2	4.5	4.7	4.6	4.4	4.2	4.3	4.4	4.4	4.4	4.4	4.5			
R88 diatexitic ultramylonite																
2.65	X	5.81	5.90	6.00	6.05	6.08	6.09	6.13	6.14	6.16	6.18	6.20	6.21	6.111	1.70	0.98
	Y	5.93	6.07	6.15	6.18	6.21	6.22	6.25	6.27	6.30	6.32	6.33	6.35	6.253	1.60	0.99
	Z	5.85	5.93	6.00	6.05	6.09	6.10	6.14	6.17	6.19	6.21	6.22	6.23	6.154	1.30	0.97
	mean V_p	5.86	5.97	6.05	6.09	6.13	6.14	6.17	6.19	6.22	6.24	6.25	6.26	6.184	1.30	0.97
	$A\%$	2.1	2.9	2.5	2.1	2.1	2.1	1.9	2.1	2.3	2.2	2.1	2.2			
M248B granitic mylonite																
2.65	X	5.86	5.98	6.06	6.11	6.13	6.15	6.17	6.19	6.20	6.21	6.23	6.24	6.157	1.40	0.98
	Y	6.06	6.16	6.23	6.26	6.27	6.29	6.31	6.32	6.34	6.35	6.36	6.38	6.299	1.30	0.97
	Z	5.83	5.97	6.05	6.08	6.11	6.13	6.15	6.16	6.18	6.19	6.20	6.21	6.150	1.00	1.00
	mean V_p	5.92	6.04	6.11	6.15	6.17	6.19	6.21	6.22	6.24	6.25	6.26	6.28	6.199	1.30	0.97
	$A\%$	3.9	3.2	3.0	2.9	2.6	2.6	2.6	2.6	2.6	2.6	2.6	2.7			
M248A gt-bi ultramylonite																
2.79	X	6.10	6.25	6.36	6.39	6.41	6.43	6.45	6.47	6.49	6.51	6.52	6.54	6.443	1.60	0.99
	Y	6.08	6.20	6.32	6.36	6.38	6.40	6.42	6.44	6.46	6.48	6.49	6.51	6.413	1.60	0.99
	Z	5.73	5.80	5.92	5.99	6.03	6.05	6.08	6.09	6.10	6.11	6.12	6.14	6.059	1.30	0.97
	mean V_p	5.97	6.08	6.20	6.25	6.27	6.29	6.32	6.33	6.35	6.37	6.38	6.40	6.303	1.60	0.99
	$A\%$	6.2	7.4	7.1	6.4	6.1	6.0	5.9	6.0	6.1	6.3	6.3	6.3			

Seismic velocities are in km/s. X = lineation; Z = normal to foliation; Y = perpendicular to lineation and parallel to foliation. $A\%$: percent anisotropy $([V_{max} - V_{min}]/V_{mean})$. $V_p = (V_p)_0 + P(dV_p/dP)$, where $(V_p)_0$ is the projected V_p in km/s for the sample at 0 MPa, and dV_p/dP is in km/s/MPa. R: correlation coefficient.

the core. Scattering is minimal because the wavelength is much greater than the average grain size of the samples. The velocities are accurate to $\pm 0.5\%$, and the precision of the measurements is better than 0.3% (Christensen and Shaw, 1970). Measurements of velocities as a function of tem-

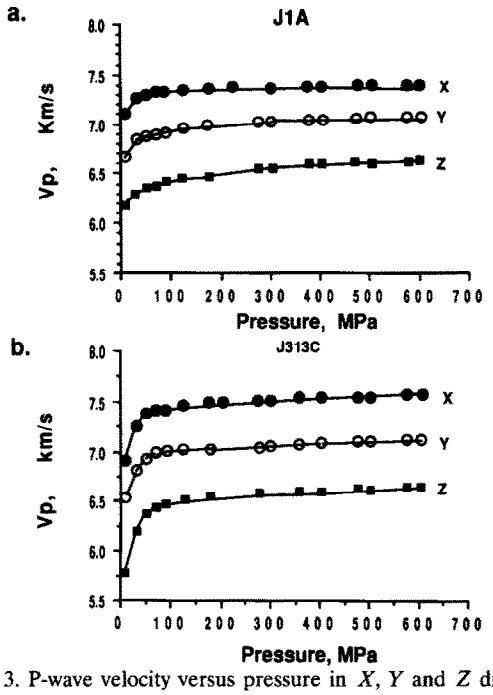

Fig. 3. P-wave velocity versus pressure in X, Y and Z directions through (a) J1A: amphibolitic ultramylonite, and (b) J313C: amphibolitic mylonite.

perature were not attempted since elastic anisotropy is not strongly temperature-dependent (Kern and Schenk, 1985 and 1988).

3.2 V_p results

V_p results for 20 high-grade mylonites are presented for various confining pressures in Table 2. All reported velocities were measured during depressurization. Velocities measured as the pressure is increased tend to be lower than those measured during depressurization below 300 MPa. This phenomenon has been attributed to the closure of microcracks at high pressure that do not completely reopen during depressurization (Birch, 1960; Gardner et al., 1965).

3.2.1 V_p–pressure relationships

The V_p–pressure curves for all samples display an initial non-linear increase in velocity at low pressures followed by a more gradual linear increase at high pressures (Fig. 3). This characteristic curve has been attributed to closure of microcracks in the samples with increasing pressure to 200–300 MPa, above which the rocks can be considered as compacted aggregates (Birch, 1960; Christensen, 1965). A comparison between sample J313C, which is medium- to fine-grained (0.1–0.8 mm), and sample J1A, which is very fine-grained (50–150 μm), suggests that the amount of rise is related to the rock microstructure, with the medium- to fine-grained mylonites exhibiting a more pronounced velocity rise than the very fine-grained ultramylonites.

The velocity–pressure relationship can be described by the linear equation:

$$V_p = (V_p)_0 + P(dV_p/dP) \quad (1)$$

where $(V_p)_0$ is the projected zero pressure velocity and dV_p/dP is the high-pressure slope. $(V_p)_0$ and dV_p/dP for each sample are given in Table 2, with dV_p/dP varying from 0.6×10^{-4} to 5×10^{-4} kms^{-1} MPa^{-1}.

3.2.2 Mean V_p

The mean V_p for each sample, which is equal to $[V(X) + V(Y) + V(Z)]/3$, is shown as a function of pressure in Figure 4. Arranged in order of decreasing average V_p at 600 MPa, the rocks can be placed in the following groups: mylonitic pyroxenite (7.79 km/s), amphibole-dominated mylonites (7.17–7.01 km/s), plagioclase-dominated mylonites (7.05–6.71 km/s) and acidic mylonites (6.42–6.20 km/s). This indicates that the lower crust has a strong lateral and vertical seismic heterogeneity (e.g., Fountain et al., 1990). The pyroxenite and amphibolitic mylonites occupy narrow, distinct high-velocity fields consistent with their narrow compositional ranges. The granitic and diatexitic mylonites have lower average V_p values, reflecting the fact that the average compressional wave velocities of quartz, K-feldspar and sodic plagioclase are similar (Babuska and Cara, 1991). The plagioclase-dominated mylonites, on the other hand, occupy a large velocity field and range from mafic to intermediate in composition.

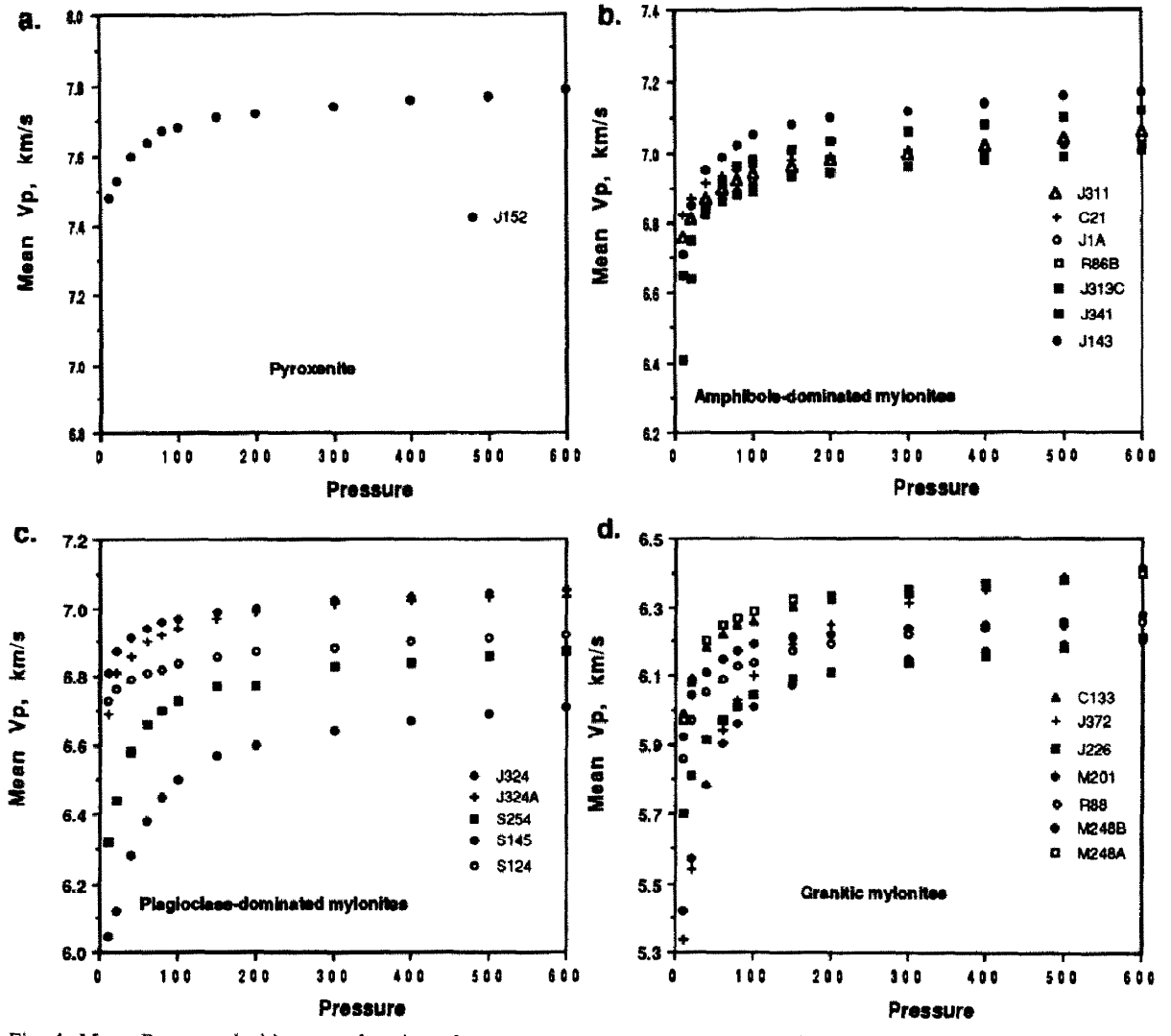

Fig. 4. Mean P-wave velocities as a function of pressure at room temperature for (a) pyroxenite; (b) amphibole-dominated mylonites; (c) plagioclase-dominated mylonites; and (d) granitic mylonites.

3.2.3 Velocity–density relationship

Figure 5 illustrates the variation of P-wave velocity among the samples due to density (ρ) and anisotropy. The dots represent the average velocities and the vertical lines, the ranges of velocity due to anisotropy at 600 MPa. The densities are those determined at room pressure since the effect of pressure on density is negligible in rocks with very low porosity ($< 1\%$). As shown in Figure 5:

$$(V_p)_{mean} = 0.937 + 2.031\rho$$

(correlation coefficient $R = 0.89$).

Although the average V_p increases roughly with increasing density, the strong anisotropy of many samples gives rise to considerable scatter in the velocity–density relationship. For example, sample J313C (an amphibolite) ranges in velocity from 6.7–7.6 km/s. Using the Nafe–Drake curve, this would correspond to a density range of 2.84–3.28 g/cm^3, which spans a range in compostion from anorthosite to peridotite. Thus considerable caution must be used in interpreting seismic data in terms of petrology because mean velocity–density relationships are non-unique (Barton, 1986; Fountain et al., 1990).

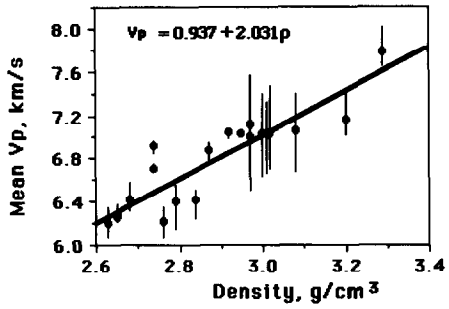

Fig. 5. Mean V_p-density relationship at 600 MPa and room temperature. Dots represent the average velocities and vertical bars show the range of V_p due to fabric-induced anisotropy in the samples. Straight line represents least-squares fit to the density and average velocity data.

3.2.4 V_p anisotropy

The coefficient of anisotropy was defined by Birch (1961) as:

$$A = 100\% \ (V_{max} - V_{min})/V_{mean} \qquad (2)$$

In many samples, A varies with pressure. Three patterns have been observed: Pattern 1: the anisotropy values for 11 samples (C21, R86B, J143, J341, J313C, J1A, J311, J372, J226, M248B and J324A) decrease progressively with increasing pressure. For example, in sample J372 the anisotropy decreases from 20.41% at 10 MPa to 4.05% at 600 MPa (Fig. 6a). This pattern is common in the amphibole-rich mylonites. The relationship between V_p anisotropy and confining pressure can be attributed to the closure of the oriented microcracks which reinforce the anisotropy due to the lattice preferred orientation (LPO) of rock-forming minerals (Ji and Salisbury, 1993). Pattern 2: the anisotropy for 3 samples (C133, S124 and J152) increases rapidly with increasing pressure in the low-pressure domain (< 150 MPa), and then decreases in the high-pressure domain (Fig. 6b). We attribute this variation to the rapid closure at low pressure of oriented cracks which oppose the anisotropy due to LPO. Pattern 3: the anisotropy for 6 samples (J324, S254, S145, R88, M201 and M248A) decreases with increasing pressure in the low-pressure domain (< 100 MPa), and then increases slightly in the high-pressure domain (100–600 MPa) (Fig. 6c). This pattern occurs in the quasi-isotropic ultramylonites. While the relationship between V_p anisotropy and confining pressure in the low-pressure domain may have the same origin as pattern 1, the slight increase of V_p anisotropy with increasing pressure probably results from differences in the pressure sensitivity of V_p in the X, Y and Z directions.

At high pressures (600 MPa), the amphibolitic mylonites show a prominent anisotropy ($A > 6\%$, mostly $> 10\%$) with an orthorhombic symmetry: $V_p(X) > V_p(Y) > V_p(Z)$. As can be seen in Figure 7, this pattern of anisotropy is different from that in mica-rich mylonites (e.g., M248A) which are

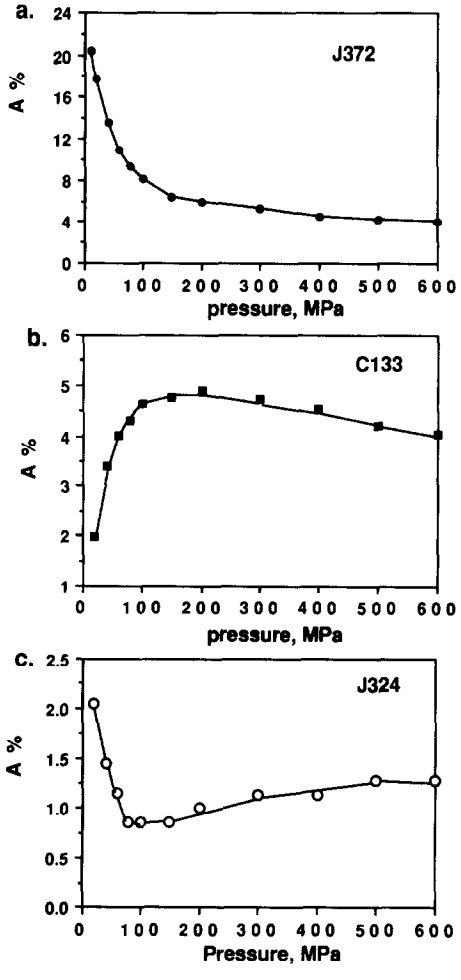

Fig. 6. V_p anisotropy versus pressure for samples J372 (a), J324 (b) and C133 (c).

transversely isotropic: $V_p(X) = V_p(Y) > V_p(Z)$ (Christensen, 1965; Burke and Fountain, 1990; Kern and Wenk, 1990; Barruol et al., 1992). Anorthositic mylonites tend to be transversely isotropic, but with $V_p(Z) > V_p(X) > V_p(Y)$, and pyroxenites tend to be fast parallel to X.

Pyroxene-bearing granulite mylonites and quartzofeldspathic (tonalitic, granitic and diatexitic) mylonites display very low values of anisotropy at high pressures (commonly $< 4\%$). These results are in good agreement with those reported by Kern and Schenk (1985, 1988), Fountain et al. (1990), Burke and Fountain (1990), Siegesmund and Kern (1990) and Braun et al. (1991).

4. Petrofabric and seismic anisotropy

The principal rock-forming minerals except garnet are strongly anisotropic (McScimin et al., 1965; Belikov et al., 1970). As shown above, however, anisotropy is not necessarily strong in polycrystalline aggregates composed of these minerals. In order to understand the origin of V_p anisotropy in the mylonites studied, we performed a systematic microstructural investigation including modal analysis (Table 1), density measurements (Table 2), petrofabic analysis and theoretical calculation of V_p contours.

4.1 Petrofabrics

Composite fabric diagrams for amphibole, plagioclase, orthopyroxene, clinopyroxene, quartz and biotite are presented for representative samples in Figures 8–12. All data are presented on equal-area, lower hemisphere projections in which the plane of projection contains the stretching lineation (X) and the pole to the foliation (Z). The fabric characteristics for each mineral are described below:

(1) Amphibole. As can be seen in Figure 8, the amphibole fabric for 5 samples (J152, J311, J1A, J143 and J372) tends to be consistent, strong and simple: the (100) planes are parallel or nearly

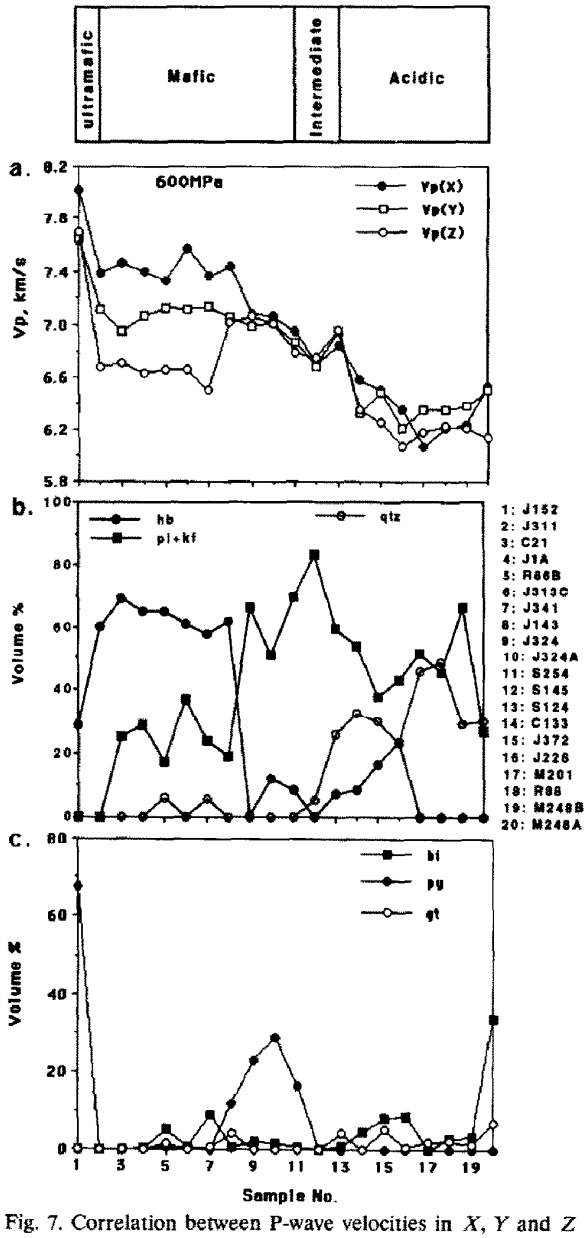

Fig. 7. Correlation between P-wave velocities in X, Y and Z directions at 600 MPa (a) and modal composition (b and c).

parallel to the XY plane, the [001] crystallographic directions have a strong concentration parallel to X and the [010] directions are parallel to Y. (110) poles define a partial girdle perpendicular to X, but the fabric is quite diffuse. The density maximum for (110) poles is always lower than that for (100) poles. For example, in sample J1A, the density maximum for amphibole (100) poles is 14.2%, whereas that for (110) poles is

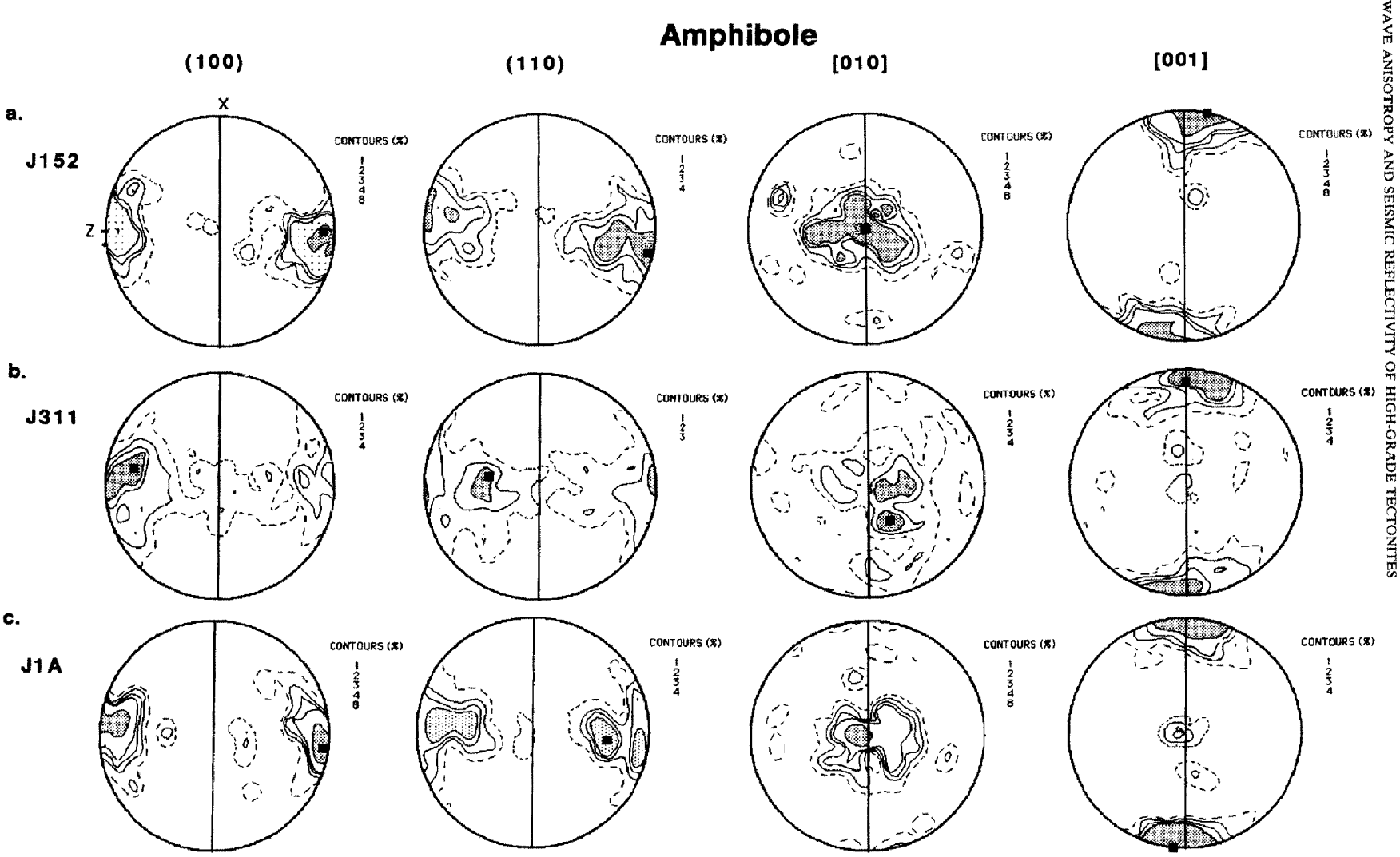

Fig. 8. Preferred orientations of hornblende (100), (110), [010] and [001] directions in samples J152 (a), J311 (b), J1A (c), J143 (d) and J372 (e). 100 measurements for J152, J1A and J372; 150 measurements for J143 and 200 measurements for J311. The *XY* plane (foliation) is the N–S solid line and is perpendicular to the page; the *X* direction (lineation) is N–S. Highest contour interval shaded. Equal-area, lower-hemisphere projection.

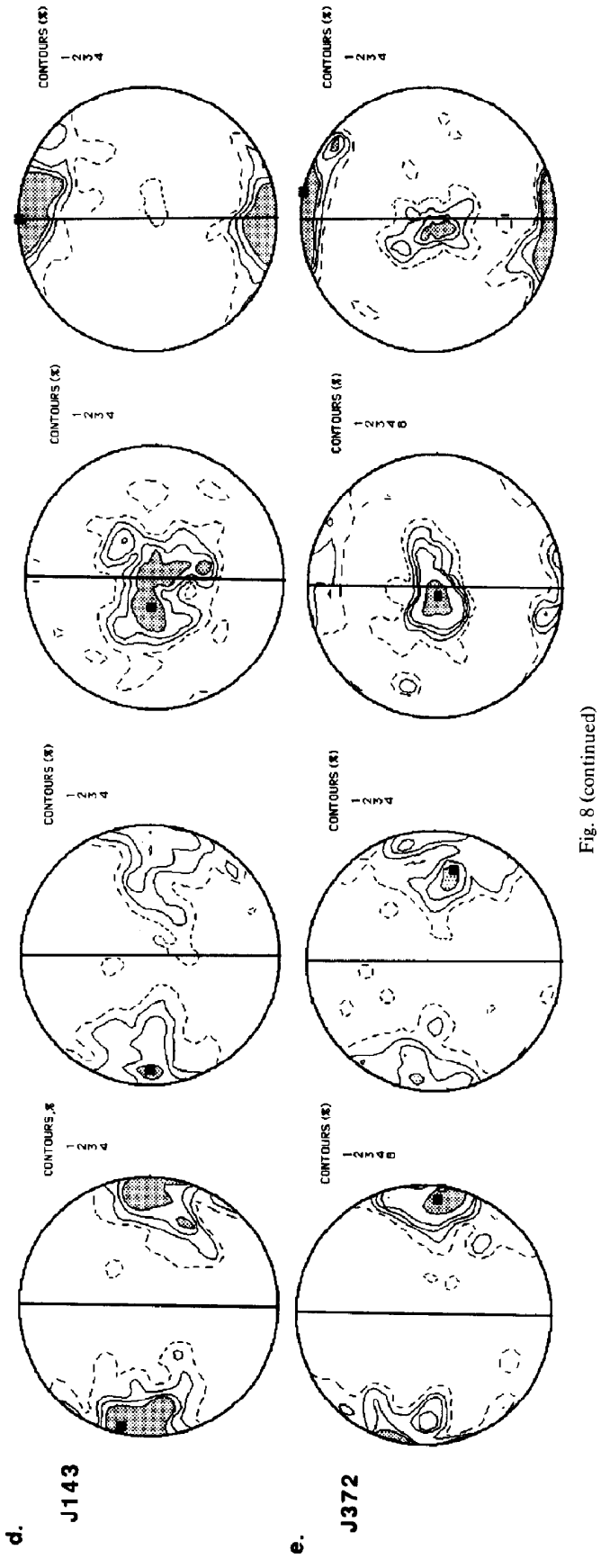

Fig. 8 (continued)

only 7.5%. Further, new grains produced by recrystallization are oriented similarly to their parent porphyroclasts (not shown here). These fabric features are consistent with those reported previously by Schwerdtner (1964), Christensen (1965), Kern (1982), Ji and Mainprice (1989), and Siegesmund et al. (1989) in middle to high-grade metamorphic rocks.

The origin of amphibole LPO deserves to be discussed. Optical and TEM observations (not shown here) suggest that the hornblende fabric in the hornblende-dominated mylonites (J311, J143, J313C) was probably produced by (100)[001] slip accommodated by recrystallization (Dollinger and Blacic, 1975; Biermann and Van Roermund, 1983; Cumbest et al., 1989; Reynard et al., 1989;

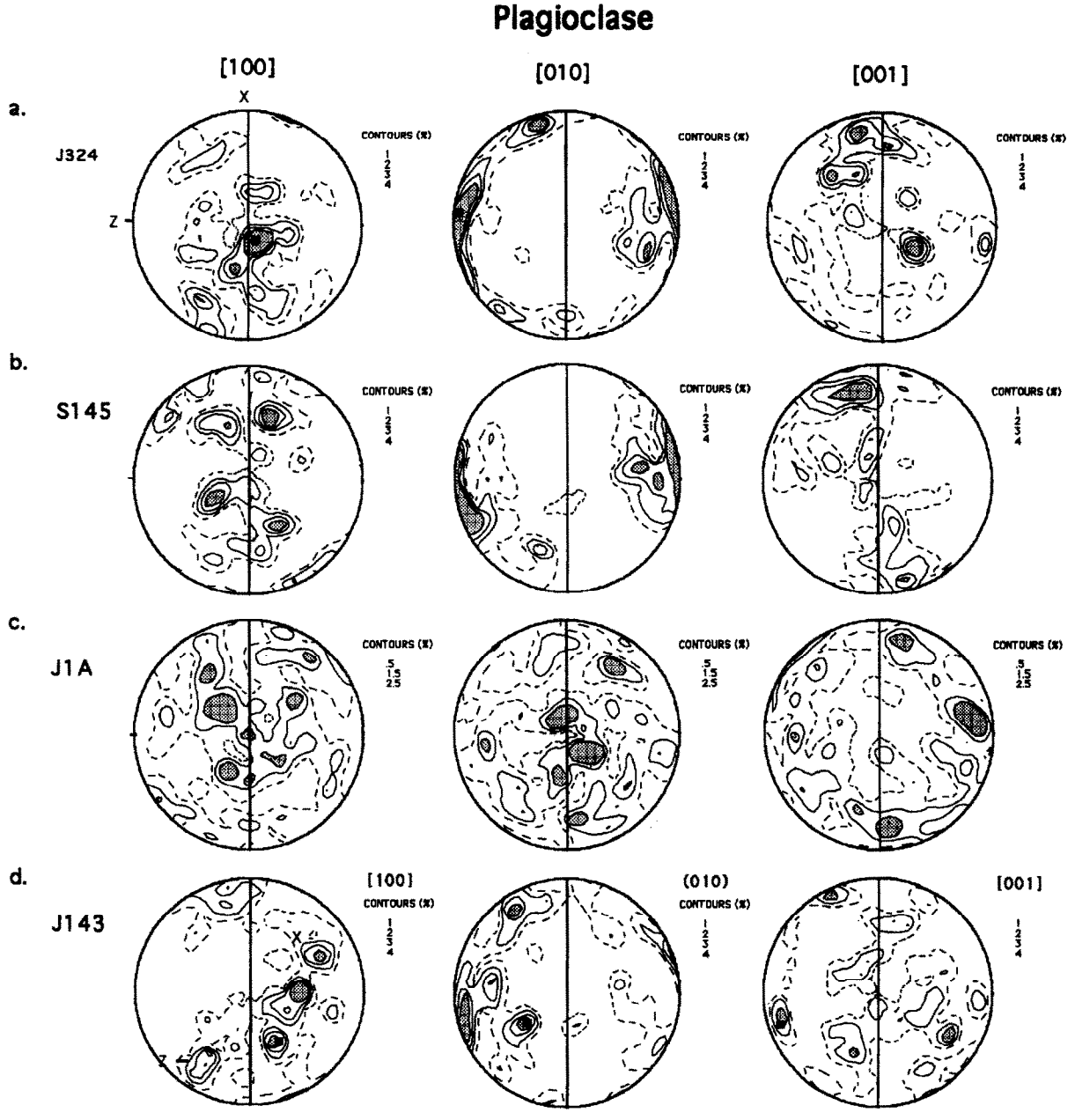

Fig. 9. Preferred orientations of plagioclase [100], (010) and [001] directions in samples J324 (a), S145 (b), J1A (c) and J143 (d). 100 measurements for J324, S145 and J143; 106 measurements for J1A. Symbols as in Fig. 8.

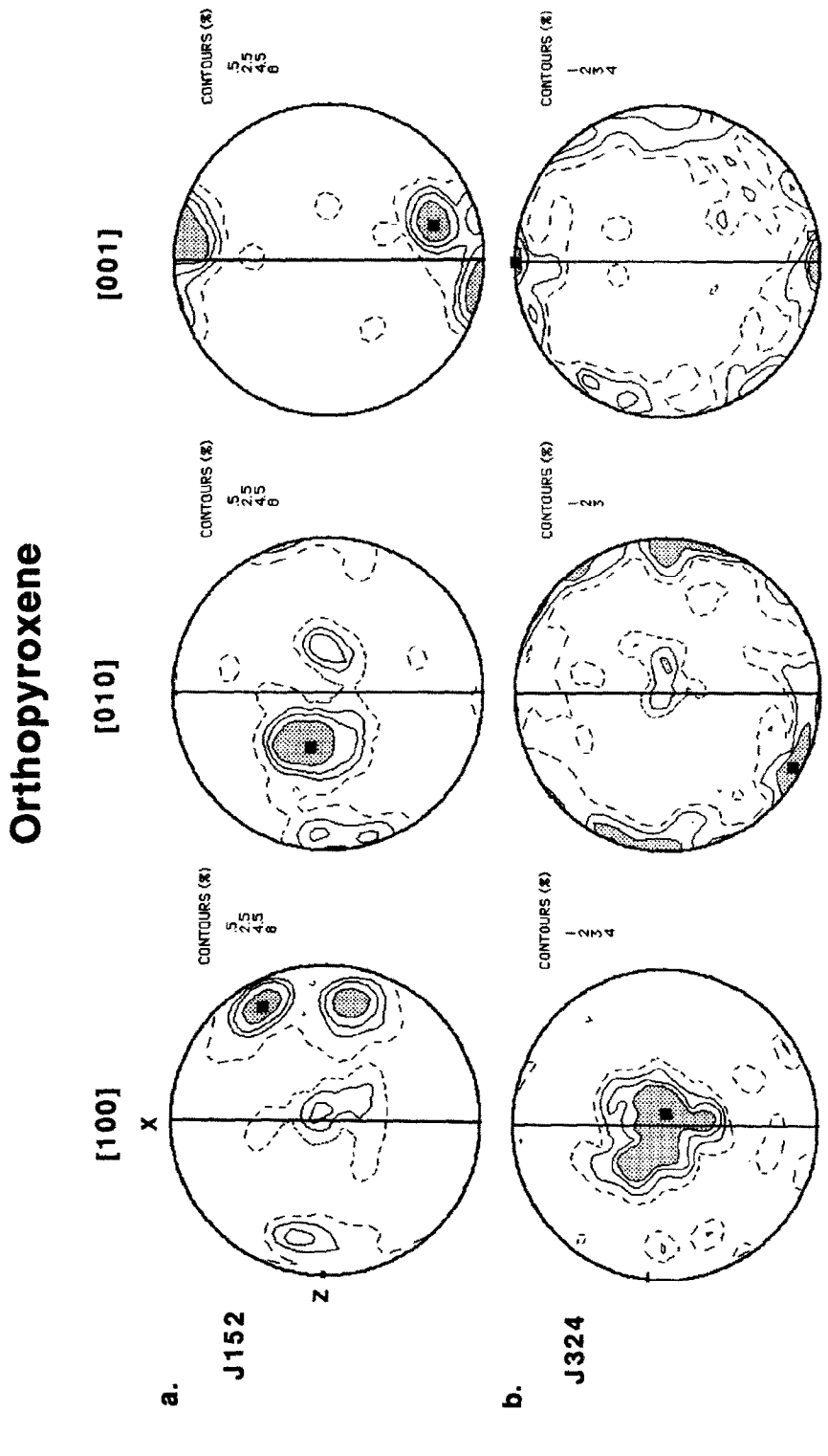

Fig. 10. Preferred orientations of orthopyroxene [100], [010] and [001] directions in samples J152 (a) and J324 (b). 127 and 140 measurements for J152 and J324, respectively. Symbols as in Fig. 8.

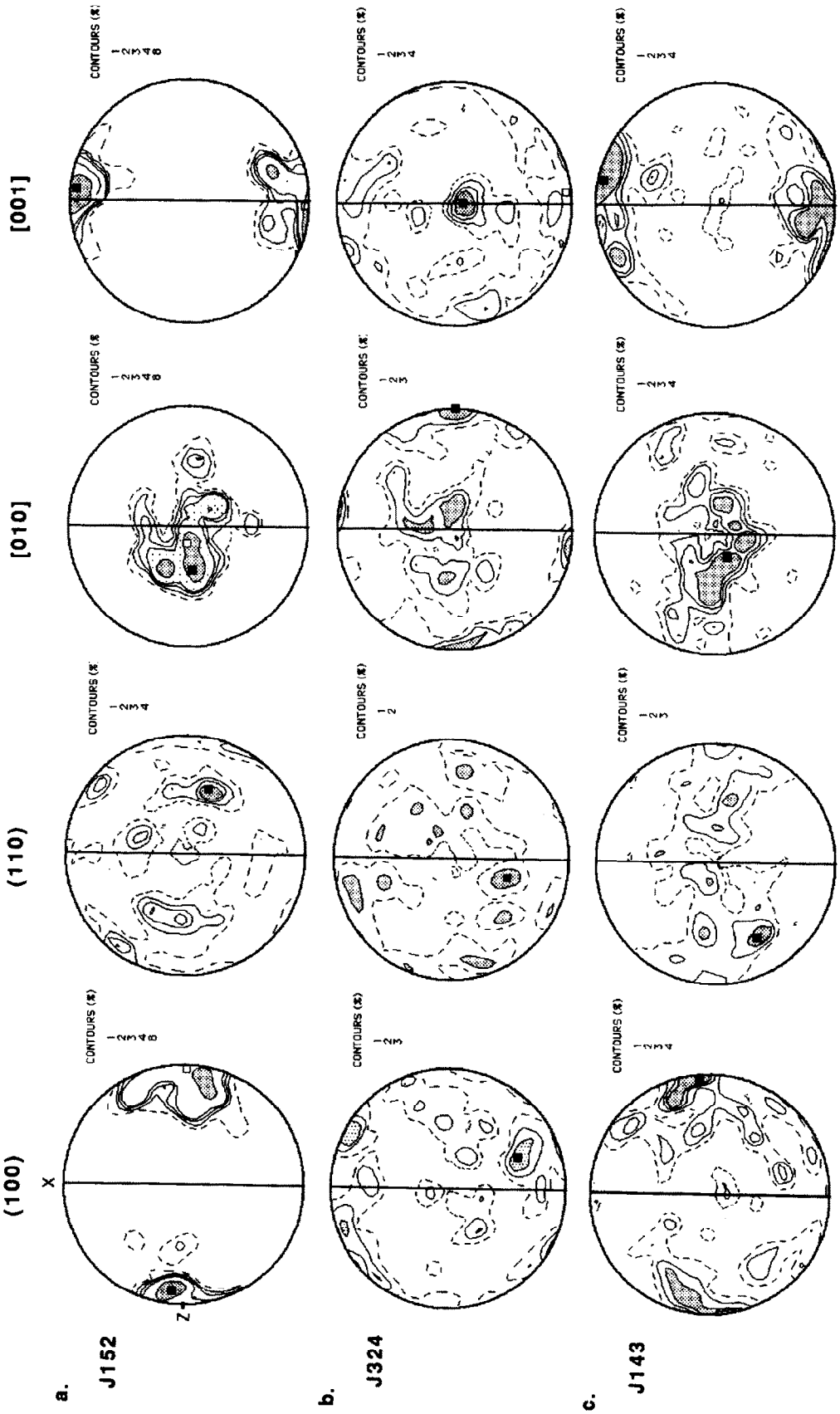

Fig. 11. Preferred orientations of clinopyroxene (100), (110), [010] and [001] directions in samples J152 (a), J324 (b) and J143 (c). 100 measurements for J152 and J143, and 113 measurements for J324. Symbols as in Fig. 8.

Skrotzki, 1990). [001] dislocations in hornblende are extensively dissociated, making recovery difficult. Eventually, dislocations pile up more easily so that recrystallization begins. It is also noted that the strong anisotropic growth capacity of amphibole leads to the development of elongate crystals under differential stress (Schwerdtner, 1964), which seems to be an important mechanism for orienting recrystallized neograins (C21, J1A and R86B). The hornblende fabric in hornblende-bearing granitic mylonites, such as J372, may be caused by simple mechanical rotation of such crystals in a ductile quartzofeldspathic matrix (Jeffery, 1922). In sample J152, hornblende nucleated and grew at the expense of orthopyroxene and clinopyroxene during retrogression from the granulite to the amphibolite facies (Fig. 2a). The orientation of the hornblende is inherited from and controlled by that of pyroxene: $(100)_{hb} \| (100)_{py}$, $[010]_{hb} \| [010]_{py}$ and $[001]_{hb} \| [001]_{py}$ (Fig. 8 and Figs. 9–10). However, whatever the orientation mechanism, the hornblende has a similar fabric pattern.

(2) Plagioclase. The plagioclase fabric seems to be sensitive to the volume fraction of plagioclase in the rock and the deformation conditions (T/P). Samples J324 and S145, in which plagioclase is volumetrically predominant (Table 1), show essentially similar LPO patterns (Fig. 9) in which (010) is subparallel to the foliation and [001] and [100] are oriented in the XY plane with [001] forming a concentration at small angles to X. This pattern of plagioclase LPO corresponds well to the fabrics reported by previous authors (Kruhl, 1987; Ji and Mainprice, 1988). The plagioclase volume fractions in samples J1A and J143 are lower, 30% and 12% respectively. The plagioclase exhibits nearly random LPO in sample J1A (Fig. 9c) which deformed under amphibolite facies conditions and only a weak concentration of (010) poles in sample J143. The above facts indicate that the development of plagioclase LPO is favoured by a high volume fraction of plagioclase in the rock and high-temperature deformation. The effect of high temperature on the development of plagioclase LPO is easy to be understood because under such conditions glide of dislocations and dynamic recrystallization can be effectively facilitated (e.g., Tullis and Yund, 1985). But why does a high content of plagioclase in the rock favour the development of plagioclase? The reasons are as follows: the matrix around the plagioclase is hornblende in the amphibolitic mylonites (J1A and J143) and pyroxene in the mafic granulite mylonite (J324). These minerals are rheologically stronger than plagioclase. A low content of these strong minerals in the rocks can increase the magnitude of stress (Handy, 1990; Ji and Zhao, in press) and enhance grain-boundary migration (dynamic recrystallization) (Prior et al., 1990) in the soft minerals and decrease grain-boundary sliding between the strong and weak grains (Starkey and Cutforth, 1978; Kronenberg, 1981).

(3) Orthopyroxene. The orthopyroxene fabrics in samples J152 and J324 are obviously different (Fig. 10). In J152, the (100) planes of orthopyroxene are subparallel to the *XY* plane and the [001] directions are parallel or subparallel to *X*. The [010] directions are oriented preferentially at a large angle to both the *X* and *Z* directions (Fig. 10). This LPO pattern for orthopyroxene is commonly observed in ultramafic complexes of upper mantle origin (e.g., Nicolas and Poirier, 1976; Christensen and Lundquist, 1982; Mercier, 1985). However, in J324, the [100] direction of orthopyroxene has a strong concentration parallel to *Y* and both the [010] and [001] directions are located in the *XZ* plane, with minor [010] and [001] concentrations parallel or subparallel to the *Z* and *X* directions, respectively (Fig. 10). This LPO pattern may be interpreted as a fabric formed firstly by (010)[001] slip (Etheridge, 1975; Nazé et al., 1987) and then diffused by recrystallization by subgrain-rotation ([100] is the axis of rotation).

(4) Clinopyroxene. Clinopyroxenes in samples J152 and J143 define a strong LPO (Fig. 11), in which [001] displays a strong preferred orientation parallel to *X*, the poles to (100) are concentrated perpendicular to the *XY* plane and the [010] directions are preferentially oriented near the *Y* direction. However, the clinopyroxene in J324 exhibits a different fabric pattern in which

the [010] axes form a girdle in the *YZ* plane with a maximum parallel to *Z*, the [001] axes are concentrated parallel to *Y* and the (100) poles are rather dispersed, but with some concentrations at small angles to the lineation. The latter clinopyroxene LPO is similar to that reported by Siegesmund et al. (1989).

(5) Quartz. As shown in Figure 12a for samples M201 and J372, quartz in the high-grade granitic, tonalitic and diatexitic mylonites displays a strong LPO with a *c*-axis maximum parallel to *Y*. This fabric pattern, which is commonly explained in terms of dislocation slip along the $< a >$ direction in the prismatic plane in quartz, is typical of high-temperature deformation (e.g., Schmid and Casey, 1986).

(6) Biotite. Biotite appears in the retrograde mylonites (e.g., M248A and J372). The (001) planes of biotite are preferentially aligned parallel to foliation (Fig. 12b).

4.2 Microstructural interpretation of V_p surfaces

In addition to measuring velocities along the *X*, *Y* and *Z* directions, we calculated complete V_p

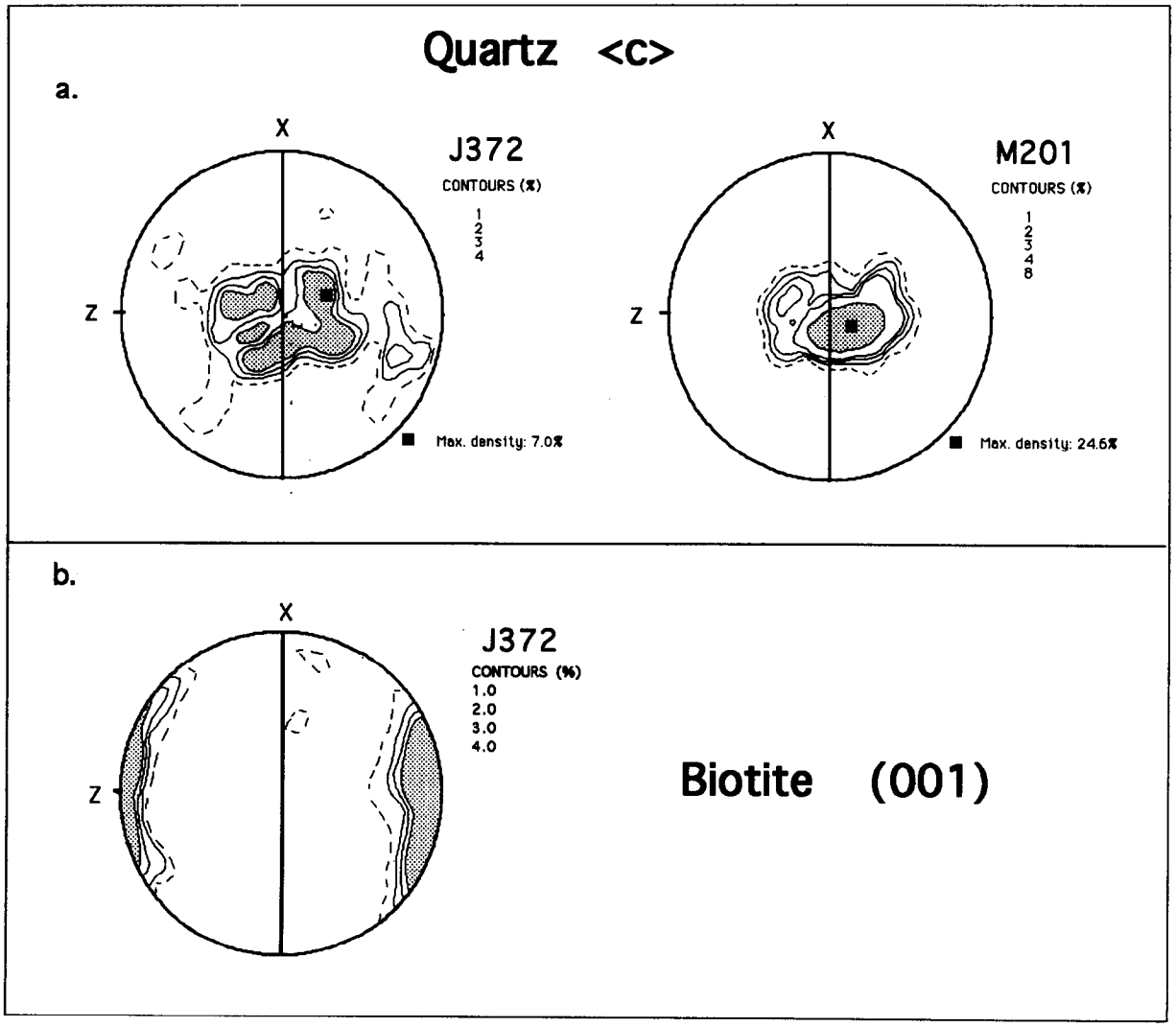

Fig. 12. C-axis fabrics of quartz in samples J372 and M201 (a), and (001) fabric of biotite in J372. 100 measurements for quartz in each sample and 150 measurements for biotite. Symbols as in Fig. 8.

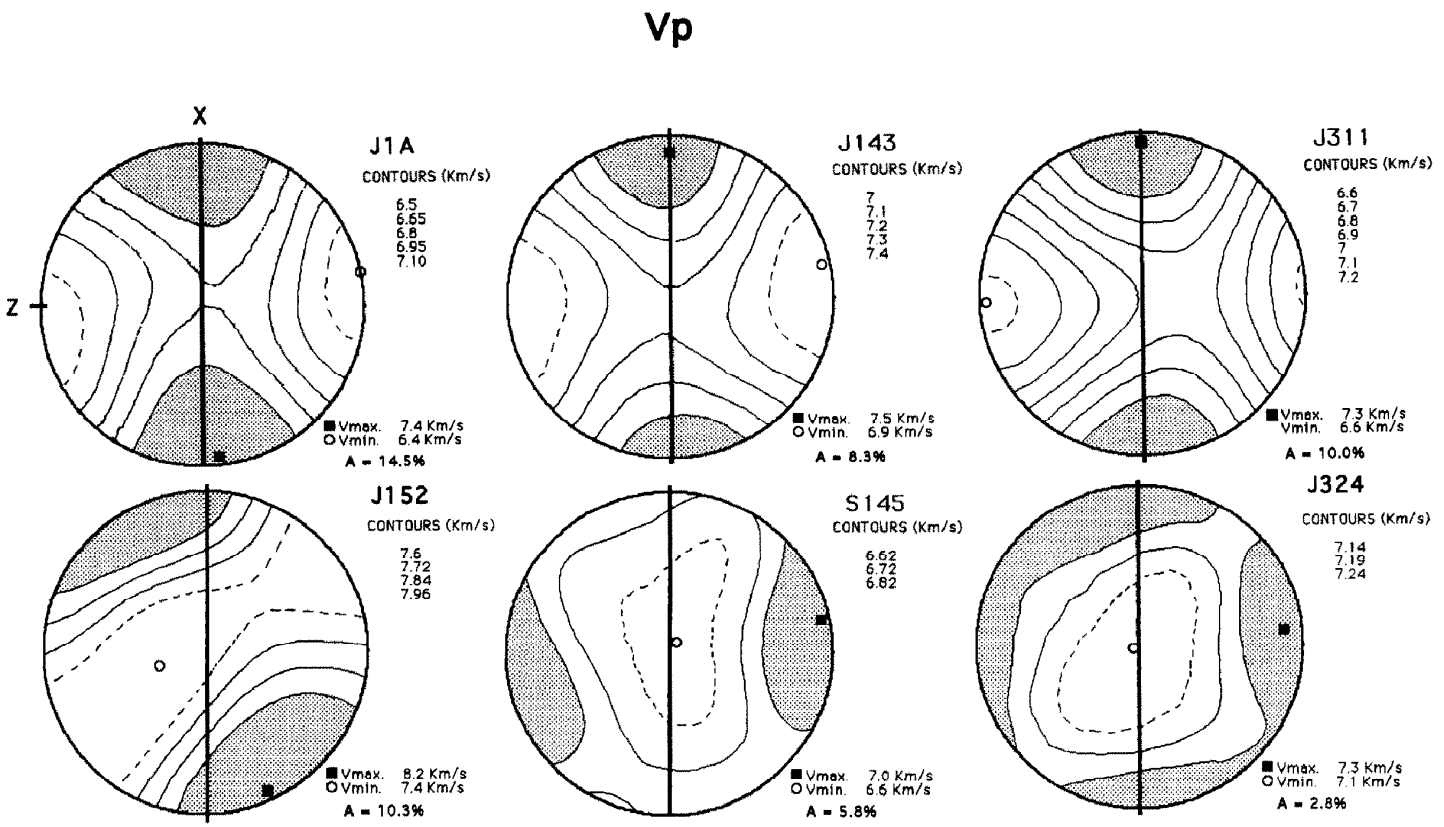

Fig. 13. Calculated V_p contours for the modal mineralogies and fabrics corresponding to samples J1A, J143 and J311 (amphibole-dominated mylonites), J152 (pyroxenite), S145 (anorthosite), and J324 (mafic ultramylonite). The foliation (XY) plane is perpendicular to the page and strikes N–S. A = anisotropy %. Equal-area, lower-hemisphere projection.

surfaces for selected samples based on the LPO, density, volume fraction and elastic stiffness coefficients of each mineral in the rocks (Crosson and Lin, 1971). The computations were performed using an interactive program (Mainprice, 1990). The Voigt average was used for seismic velocity calculation because it gives the closest agreement between LPO-derived and laboratory-measured seismic velocities (Seront et al., 1989). The calculated velocities pertain to conditions of one atmosphere pressure, room temperature and zero porosity, and must be compared with velocities measured at a pressure high enough to close microcracks (Christensen, 1965).

4.2.1 Amphibole-dominated mylonites

As shown in Figure 13, the calculated results are very comparable to those determined experimentally at 500 MPa in the amphibolitic ultramylonite (J1A), clinopyroxene and garnet-bearing amphibolite (J143) and mylonitic hornblendite (J311). The fastest, intermediate and slowest P-wave velocities are in the X, Y and Z directions, respectively. The V_p anisotropy coefficients determined for J1A, J143 and J311 are high, 14.5%, 8.3% and 10.0%, respectively, for the calculated velocities at room pressure, and 11.0%, 6.0% and 9.9% for the measured velocities at 500 MPa (Table 2). The differences between the calculated and measured anisotropies may be attributed to the presence of minor constituents such as sericite and opaques. The highest V_p is parallel to the lineation (X) because the [001] direction of hornblende, which is close to the fastest V_p direction in single crystal hornblende (Belikov et al., 1970), is oriented parallel to the lineation in all three samples. The velocities are intermediate and slowest in the Y- and Z-directions, because the intermediate and slowest P-wave directions in hornblende single crystals ([010], (100)) are oriented parallel to the Y- and Z-directions, respectively (Fig. 8). It is noteworthy that the presence of plagioclase and particularly, pyroxene and garnet, always diminish the fabric-induced anisotropy caused by hornblende.

4.2.2 Pyroxene-dominated rocks

The calculated P-wave velocities in the X, Y and Z directions in the mylonitic pyroxenite (J152) are 8.00, 7.50 and 7.72 km/s, respectively (Fig. 13). These values are in very good agreement with the measured values at 500 MPa: $V_p(X) = 8.00$ km/s, $V_p(Y) = 7.63$ km/s and $V_p(Z) = 7.68$ km/s (Table 2). It is important to note that the calculated V_p surfaces are asymmetric with repect to the structural elements (i.e., the foliation and lineation). Thus the highest V_p is not parallel to the lineation, but lies about 20° to it. Accordingly, the anisotropy calculated from the experimentally measured velocities (5.0%) does not represent the maximum anisotropy (10.3%) in the specimen.

4.2.3 Plagioclase-dominated rocks

(1) Anorthosite. Figure 13 shows the calculated V_p surface for a hypothetical pure plagioclase aggregate with the LPO of sample S145 (Fig. 9). The anisotropy coefficient is 5.8% with the fastest (7.00 km/s), intermediate (6.75 km/s) and slowest (6.60 km/s) P-wave velocities near the Z, X and Y directions, respectively. The measured P-wave velocities along the Z, X and Y directions at 500 MPa are 6.73, 6.68 and 6.66 km/s, respectively. Both the calculated and measured results show a similar V_p pattern with $V_p(Z) > V_p(X) > V_p(Y)$. This pattern reflects the concentration of high-velocity (010) poles perpendicular to foliation and the tendency for the low-velocity [101] and [100] axes to lie in the foliation plane. However, the measured bulk anisotropy is much lower than the calculated one. This is attributed to the presence of sericite (10%) and quartz (5%) in the mylonitic anorthosite. Optical observation shows that the quartz grains have their c-axes preferentially parallel to the Y direction, causing V_p to increase in this direction as the fast V_p direction in quartz is parallel to the c-axis (McScimin et al., 1965). The influence of the sericite on velocites is difficult to assess quantitatively because its elastic constants have not yet been determined and the LPO of sericite cannot be measured optically due to its small grain size. Assuming that the sericite grains have similar elastic properties and LPO patterns to muscovite, we would expect that alteration of plagioclase to sericite might decrease V_p in the direction normal to the foliation. As a

result, the presence of sericite and quartz in the anorthosite would result in attenuation of the seismic anisotropy caused by the LPO of plagioclase. Thus, the calculated P-wave velocities may be more representative of the properties of mylonitic anorthosite under lower crustal conditions than measured velocities since sericite is of course absent in the lower crust.

(2) Mafic ultramylonites. It is surprising that the V_p anisotropy coefficient in the strongly deformed mafic ultramylonite sample (J324) is very low, 2.8% and 1.3% for the calculated and measured values, respectively (Fig. 13 and Table 2). Experimental measurements show, however, that other mafic mylonites (J324A and S254) consisting of plagioclase, clinopyroxene and orthopyroxene are also quasi-isotropic ($A < 2.5\%$). The contributions of plagioclase, clinopyroxene and orthopyroxene evidently cancel one another to produce low values of V_p anisotropy. It should be noted that $V_p(X) = V_p(Z) > V_p(Y)$ for sample J324, whereas $V_p(X) > V_p(Y) > V_p(Z)$ for J324A and S254 (Fig. 7 and Table 2). To explain this discrepancy, we suggest that the presence of hornblende is a contributing factor to the anisotropy in samples J324A (12% hb) and S254 (8.5% hb).

4.2.4 Quartzofeldspathic mylonites

The V_p properties (Table 2) in the diatexitic (M201, R88 and M248B) and tonalitic (S124) ultramylonites are dominated by the LPO of quartz (Fig. 12), and strongly attenuated by the LPO of K-feldspar, resulting in low anisotropy. However, the V_p properties in the hornblende- and biotite-bearing granitic mylonites (e.g., J372 and J226) are dominated by hornblende and biotite, both of which are strongly anisotropic as single crystals and strongly aligned in the mylonites (Figs. 8 and 12). The summed contribution of feldspar and quartz to the V_p anisotropy is negligible because they oppose each other. We can explain the V_p distribution in samples M248A and C133 in a similar way. M248A, which contains 34% biotite, is fast parallel to foliation and slow perpendicular to it (Table 2), because the biotite (001) planes are preferentially aligned parallel to the foliation (Fig. 11b). In sample C133, which contains only 9% hornblende and 5% biotite, the contribution of hornblende and biotite does not appear to be large enough to offset that of plagioclase (54%).

In summary, the measurements and microstructural analyses discussed above show that amphibolitic mylonites exhibit significant V_p anisotropy, whereas mafic granulite mylonites and quartzofeldspathic (tonalitic, granitic and anatexitic) mylonites and ultramylonites are quasi-isotropic ($A < 4\%$), despite their intensive plastic deformation under granulite facies conditions. The opposing contributions of different oriented minerals is thought to be the most important factor in the attenuation of V_p anisotropy in mafic granulite mylonites and quartzofeldspathic mylonites. It has been shown that intracrystalline slip is the most important mechanism for the formation of LPO (Wenk and Christie, 1991). Unlike face-centered-cubic metals, pyroxene, amphibole, feldspar and quartz do not have five independent slip systems to accommodate an arbitrarily imposed deformation by slip alone (Mainprice and Nicolas, 1989). These minerals deform by slip on only one or two easiest slip planes and directions, with dynamic recrystallization serving as a possible accommodation mechanism (Drury and Urai, 1990; Ji and Mainprice, 1990). In plagioclase, (010)[001] is the dominant dislocation slip system under high-grade metamorphic conditions (Olsen and Kohlstedt, 1984; Montardi and Mainprice, 1987; Ji and Mainprice, 1988). Prism $<a>$ slip is considered the main deformation mechanism in natural quartz under upper amphibolite and granulite facies conditions, although prism $<c>$ slip has been found in special cases (Mainprice et al., 1986). (100)[001] is the dominant slip system in both ortho- and clinopyroxene (Mercier, 1985; Doukhan et al, 1986) in granulites and pyroxenites. (100)[001] also appears to be the dominant slip system in amphibole. In polycrystalline aggregates (rocks), where grains deform under the influence of a single dominant slip system, the fabric is the result of the alignment of the slip planes and directions, respectively, with the shear plane and direction during progressive rotational deforma-

TABLE 3

Reflection coefficients at the interfaces between undeformed rocks

Lithology	pyroxenite (J152)	amphibolite (J313C)	mafic granulite (J324)	anorthosite (S145)	tonalite (C133)	granite (J226)	diatexite (M248B)
Mean V_p (km/s)	7.79	7.12	7.05	6.71	6.42	6.21	6.28
Density (g/cm^3)	3.29	2.97	2.92	2.74	2.68	2.76	2.65
Impedance (10^{-6} kgm^{-2} s^{-1})	25.63	21.15	20.59	18.39	17.21	17.14	16.64
pyroxenite	0.000	*0.096*	**0.109**	**0.164**	**0.197**	**0.199**	**0.213**
amphibolite		0.000	0.013	*0.070*	**0.103**	**0.105**	**0.119**
mafic granulite			0.000	*0.056*	*0.089*	*0.091*	**0.106**
anorthosite				0.000	0.033	0.035	*0.050*
tonalite					0.000	0.002	0.017
granite						0.000	0.015
diatexite							0.000

Reflection coefficients derived from densities and mean velocities at 600 MPa. Bold-type values: $R_c \geqslant 0.100$; italicised values: $0.050 \leqslant R_c < 0.100$; normal-type values: $R_c < 0.050$. Values + or − depending on juxtaposition of lithologies.

tion (Ribe, 1989; Ribe and Yu, 1991). In the case of large deformation, the shear plane and direction are nearly parallel, respectively, to the foliation and lineation in the mylonites. Therefore, ductile deformation is expected to cause the (010) planes of plagioclase (high V_p), the (100) planes

TABLE 4

Reflection coefficients at the interfaces between mylonites in the Snowbird Tectonic Zone

Lithology	mylonitic pyroxenite (J152)	amphibolitic mylonite (J313C)	mafic mylonite (J324)	anorthositic mylonite (S145)	tonalitic mylonite (C133)	granitic mylonite (J226)	diatexitic mylonite (M248B)
$V_p(Z)$ (km/s)	7.70	6.66	7.07	6.75	6.35	6.07	6.21
Density (g/cm^3)	3.29	2.97	2.92	2.74	2.68	2.76	2.65
Impedance (10^{-6} kgm^{-2}s^{-1})	25.33	19.78	20.64	18.50	17.02	16.75	16.46
mylonitic pyroxenite	0.00	**0.123**	**0.100**	**0.149**	**0.196**	**0.204**	**0.212**
amphibolitic mylonite		0.000	0.021	0.033	*0.075*	*0.083*	**0.100**
mafic mylonite			0.000	*0.055*	*0.096*	**0.104**	**0.113**
anorthositic mylonite				0.000	0.042	*0.050*	*0.058*
tonalitic mylonite					0.000	0.008	0.017
granitic mylonite						0.000	0.009
diatexitic mylonite							0.000

Absolute reflection coefficients derived from densities and velocities measured normal to foliation.
Bold-type values: $R_c \geqslant 0.100$; italicised values: $0.050 \leqslant R_c < 0.100$; normal-type values: $R_c < 0.050$.
Values + or − depending on juxtaposition of lithologies.

of clinopyroxene (low-moderate V_p), the (100) planes of amphibole (low V_p), {*m*} of quartz (low V_p) all to become aligned parallel or subparallel to foliation. Accordingly, their summed contributions tend to attenuate V_p anisotropy.

5. Reflectivity of high-grade tectonites

5.1 Influence of fabric-induced anisotropy on the reflectivity of lithological interfaces

In order to investigate the effect of fabric-induced anisotropy on the reflectivity of lithologic interfaces, we calculated the reflection coefficient (Rc) at the contact between two mylonites and between their isotropic protoliths, respectively, from the relation:

$$R_c = (\rho_1 V_1 - \rho_2 V_2)/(\rho_1 V_1 + \rho_2 V_2) \quad (3)$$

where ρ_1 and ρ_2 are the densities of rocks 1 and 2, and V_1 and V_2 are the velocities of rocks 1 and 2, respectively. The velocities measured normal to foliation [$V_p(Z)$] in the mylonites were used to simulate near-vertical ray propagation, assuming for the moment that the foliation is approximately horizontal. The velocities in the protoliths were represented by the mean velocity of the respective mylonite samples. Assuming that the rock density of the rocks did not change during mylonitization (e.g., Kern and Wenk, 1990), the absolute values of the calculated reflection coefficients in the above two cases are given in Tables 3 and 4, respectively.

Not surprisingly, lithologic contrast is the most important factor affecting reflectivity. An examination of Table 3 shows that:

(1) In the Snowbird tectonic zone, the largest reflection coefficients (Rc = 0.096–0.213) would be associated with interfaces between pyroxenite and its wall rocks, implying that sufficiently large lenticular inclusions of pyroxenite in ductile layers of the lower crust can cause strong reflections.

(2) Tonalite-granite, granite-diatexite, and tonalite-diatexite contacts have very low reflection coefficients ($R_c < 0.02$).

(3) Mafic dykes (isotropic amphibolites) are very good reflectors ($R_c > 0.100$) against acidic and intermediate rocks such as tonalite, granite and diatexite, but are almost transparent against mafic granulites ($R_c = 0.013$).

TABLE 5

Reflection coefficients at the interfaces between undeformed rocks and mylonites

Lithology		pyroxenite (J152)	amphibolite (J313C)	mafic granulite (J324)	anorthosite (S145)	tonalite (C133)	granite (J226)	diatexite (M248B)
	Impedance (10^{-6} $kgm^{-2}s^{-1}$)	25.63	21.15	20.59	18.39	17.21	17.14	16.64
mylonitic pyroxenite	25.33	0.006	0.090	0.103	0.159	0.191	0.193	0.207
amphibolitic mylonite	19.78		0.033	0.020	0.036	0.069	0.072	0.086
mafic mylonite	20.64			0.001	0.058	0.091	0.093	0.107
anorthositic mylonite	18.50				0.003	0.036	0.038	0.053
tonalitic mylonite	17.02					0.006	0.004	0.011
granitic mylonite	16.75						0.012	0.003
diatexitic mylonite	16.46							0.005

Reflection coefficients derived from densities and velocities measured normal to foliation at 600 MPa, assuming underformed rock overlies mylonite.

(4) The interfaces between mafic granulites (pyriclasites) and intermediate or acidic rocks also have high reflection coefficients ($R_c \geqslant 0.089$), whereas coefficients at the contacts between anorthosite and the other lithologies examined are moderate.

While seismic reflectivity is largely controlled by lithologic contrasts, it is clear from a comparison of Tables 3, 4 and 5 that fabric-induced anisotropy can either enhance or decrease reflectivity. For example, anisotropy increases the reflection coefficient by 62% at the interface between amphibolitic mylonite and mafic mylonite, whereas it decreases by 27% at the interface between amphibolitic mylonite and tonalitic mylonite. In both cases, the changes in reflectivity are caused by the introduction of oriented hornblende. Although the mean velocity of the amphibolite is comparable to that of the mafic granulite, and higher than that of the tonalite and granite, the P-wave velocity normal to the foliation in the amphibolitic mylonite is significantly lower than that in the mafic mylonite and almost equivalent to the fast velocites in the tonalitic and granitic mylonites (Fig. 7).

Therefore, lithological variation, modified by fabric-induced anisotropy, should be an important source of reflections in the lower crust. Strong reflections correspond to interfaces between any combination of mafic or ultramafic rocks on the one hand and acidic or intermediate rocks on the other. These reflections can be enhanced or muted, however, by the effects of lattice preferred orientation (Christensen, 1989).

5.2 Reflectivity of mylonite zones without lithological contrast

Assuming that a given mylonite has the same density and mineral composition as its protolith (Kern and Wenk, 1990), the reflection coefficient due to mylonitization alone for propagation normal to foliation can be calculated from the relation:

$$R_c = \left[V_p(Z)\rho - V_{p_{mean}}\rho\right] / \left[V_p(Z)\rho + V_{p_{mean}}\rho\right]$$
$$= \left[V_p(Z) - V_{p_{mean}}\right] / \left[V_p(Z) + V_{p_{mean}}\right] \qquad (4)$$

and the maximum and minimum coefficients can be calculated, respectively, by substituting V_{max}

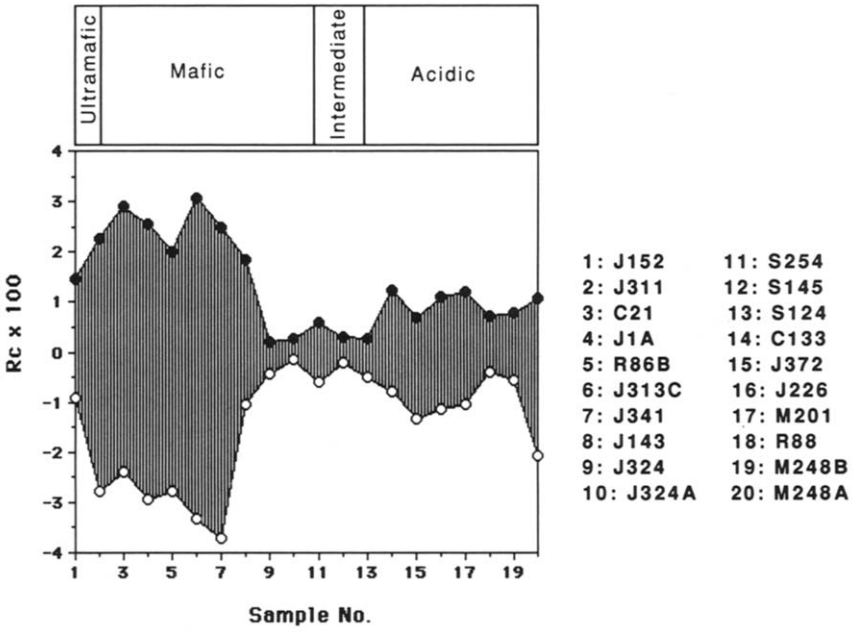

Fig. 14. Range of reflection coefficients at the boundary between a mylonite and its undeformed protolith. Values calculated from densities and velocities at 600 MPa.

and V_{min} for $V_p(Z)$ in eq. 4. As can be seen in Table 5 and Figure 14, the absolute value of R_c induced by velocity anisotropy alone is larger than 0.02 only for amphibolitic mylonites. Synthetic seismogram modelling requires reflection coefficients of around 0.10 to produce strong reflectors (Warner, 1990), but fair reflections can be produced by interfaces with coefficients of 0.04 (Sheriff, 1975). As pointed out by Fountain et al. (1984), constructive interference in layered mylonitized/unmylonitized zones can double and sometimes triple the peak-to-trough amplitude of a complex reflection so that appreciable reflections can arise even if acoustic contrasts are small. Thus, anisotropic effects can enhance or mute reflections, but in general, are not strong enough to cause them, except possibly in the case of amphibolites and micaceous rocks.

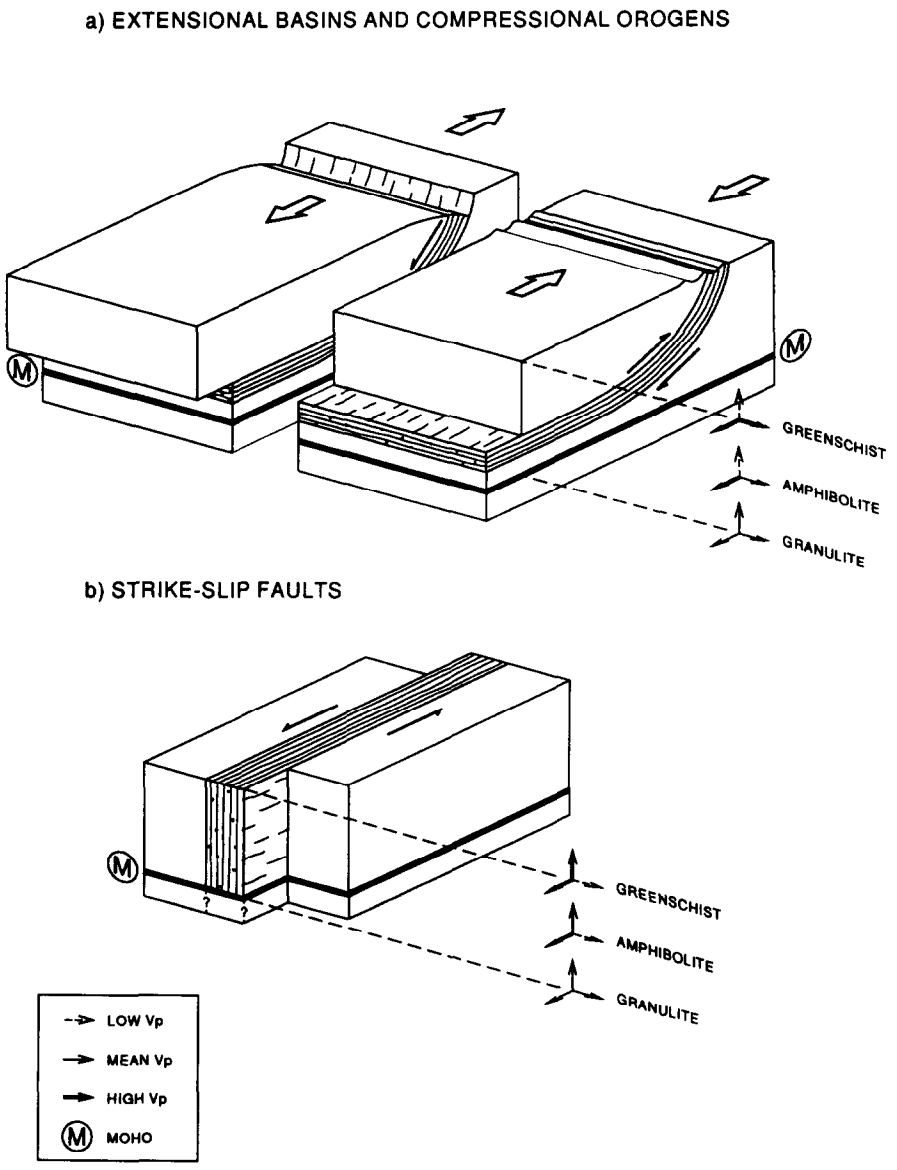

Fig. 15. Structural settings conducive to V_p anisotropy due to lattice preferred orientation. If sufficiently large volumes of the crust are involved, regional anisotropy may be present.

6. Discussion: possible kinematic implications of seismic anisotropy

While most of the common rock-forming minerals are anisotropic, it is clear from the preceeding discussion that micas and amphiboles are the most likely to cause seismic anisotropy. As can be seen in Figure 15, seismic anisotropy and thus exhanced or muted reflectivity caused by LPO of such minerals, might be anticipated at several levels of the crust along major strike-slip faults and crust-cutting shear zones underlying extensional terranes and compressional orogens, provided appropriate lithologies are intercepted by these shear zones, that these lithologies are at the right metamorphic grade and that sufficiently large volumes of rock are involved to be seismically detectable.

Although the same rules will dictate whether anisotropy exists at a given level of a crustal shear zone, regardless of tectonic setting, the setting determines its orientation. For example, large-scale strike-slip fault zones (e.g., the Red River fault in China and the Great Slave Lake fault in Canada) in which intensive ductile deformation produced 5–25-km-wide mylonites with steeply dipping foliation and horizontal extension lineation, will be transversely anisotropic at mid-crustal levels, with V_p fast parallel to the fault and slow perpendicular, if the fault zones intersect phyllosilicate-rich greenschist facies rocks in the middle crust, and amphibole-rich amphibolite facies rocks in the upper part of the lower crust. At deeper levels, however, where the fault lies in the pyroxene granulite facies, the fault zone lithologies may be quasi-isotropic in V_p.

In the subhorizontal shear zones underlying extensional basins and compressional orogens, the anisotropy, if present, will be similar in origin, but V_p is expected to be transversely isotropic in greenschist facies levels of the crust and transversely anisotropic in amphibole-facies levels, with V_p slow in the vertical direction for both levels. As before, fault zones in the granulite facies lower crust should be quasi-isotropic. As the fault zone approaches the surface and steepens, the anisotropy pattern will be rotated about an axis perpendicular to the extension lineation, causing V_p to be slow perpendicular to foliation when the dip becomes steep.

Continuous fault zones in the continental crust are likely to appear discontinuous in seismic reflection profiles due to lateral and vertical changes in lithological composition, metamorphic grade and seismic anisotropy. Where large volumes of the crust are deformed, however, as in collision orogenic zones and as has been suggested for reflective lower crust (e.g., Barazangi and Brown, 1986), the anisotropy patterns discussed above should be generally applicable and detectable even by refraction. Although V_p anisotropy related to LPO has been observed in the continental crust (e.g., Brocher and Christensen, 1990), such observations are still uncommon. As in the ocean basins, where upper mantle anisotropy was documented from azimuthal refraction experiments (e.g., Raitt et al., 1969; Keen and Barrett, 1971), anisotropy is only likely to be documented in the continental crust from refraction experiments and shear wave splitting measurements which have been carefully designed to look for it.

Acknowledgments

S. Ji would like to thank NSERC for research grant OGP0121552 and the post-doctoral fellowship under which this study was initiated. We thank Drs. J. Martignole, T. Frisch and W. Trzcienski for helpful discussion of the manuscript, Drs. S. Karato and H.R. Wenk for constructive reviews and R.J. Iuliucci for technical assistance in the laboratory. We also wish to acknowledge the financial support from Petro Canada and NSERC which made it possible to establish the High Pressure Laboratory at Dalhousie University and the continuing support provided by NSERC and the Geological Survey of Canada which has made it possible to maintain the facility.

References

Babuska, V. and Cara, M., 1991. Seismic Anisotropy in the Earth. Kluwer, Dordrecht, 217 pp.

Barazangi, M. and Brown, L. (Editors), 1986. Reflection Seismology: The Continental Crust. Am. Geophys. Union, Geodyn. Ser. Vol. 14, Washington, D.C., 339 pp.

Barruol, G., Mainprice, D., Kent, H., de Saint Blanquat, M. and Compte, P., 1992. 3D seismic study of a ductile shear zone from laboratory and petrofabric data (le Saint Barthélémy Massif, Northern Pyrénées, France). Terra Nova, 4: 63–76.

Barton, P.J., 1986. The relationship between seismic velocity and density in the continental crust — a useful constraint? Geophys. J.R. Astron. Soc., 87: 195–208.

Belikov, P., Alexandrov, K.C. and Ryshova, T.V., 1970. Elastic Properties of Rock-forming Minerals and Rocks. Nauka, Moscow, 275 pp.

Biermann, C. and van Roermund, H.L.M., 1983. Defect structures in naturally deformed clinoamphiboles — a TEM study. Tectonophysics, 95: 267–278.

Birch, F., 1960. The velocity of compressional waves in rocks to 10 kilobars. 1. J. Geophys. Res., 65: 1083–1102.

Birch, F., 1961. The velocity of compressional waves in rocks to 10 kilobars. 2. J. Geophys. Res., 66: 2199–2224.

Braun, G., Siegesmund, S. and Dahms, M., 1991. The influence of quartz textures on the seismic anisotropy in lower crustal granulites. J. Struct. Geol., 13(8): 955–966.

Brocher, T.M. and Christensen, N.I., 1990. Seismic anisotropy due to preferred mineral orientation observed in shallow crustal rocks in southern Alaska. Geology, 18: 737–740.

Burke, M. and Fountain, D.M., 1990. Seismic properties of rocks from an exposure of extended continental crust: new laboratory measurements from the Ivrea zone. Tectonophysics, 182: 119–146.

Christensen, N.I., 1989. Reflectivity and seismic properties of the deep continental crust. J. Geophys. Res., 94(B12): 17,793–17,804.

Christensen, N.I., 1965. Compressional wave velocities in metamorphic rocks at pressures to 10 kilobars. J. Geophys. Res., 70(24): 6147–6164.

Christensen, N.I. and Fountain, D.M., 1975. Constitution of the lower continental crust based on experimental studies of seismic velocities in granulite. Geol. Soc. Am. Bull., 86: 227–236.

Christensen, N.I. and Lundquist, S.M., 1982. Pyroxene orientation within the upper mantle. Geol. Soc. Am. Bull., 93: 279–288.

Christensen, N.I. and Shaw, G.H., 1970. Elasticity of mafic rocks from the Mid-Atlantic Ridge. Geophys. J., 20: 271–284.

Christensen, N.I. and Szymanski, D.L., 1988. Origin of reflections from the Brevard fault zone. J. Geophys. Res., 93: 1087–1102.

Crosson, R.S. and Lin, J.W., 1971. Voigt and Reuss prediction of anisotropic elasticity of olivine. J. Geophys. Res., 76: 570–578.

Cumbest, R.J., Drury, M.R., van Roermund, H.L.M. and Simpson, C., 1989. Dynamic recrystallization and chemical evolution of clinoamphibole from Senja, Norway. Contrib. Mineral. Petrol., 101: 339–349.

Dollinger, G. and Blacic, J.D., 1975. Deformation mechanisms in experimentally and naturally deformed amphiboles. Earth Planet. Sci. Lett., 26: 409–416.

Doukhan, J.C., Doukhan, N., Nazé, L. and Van Duysen, J.C., 1986. Défauts de réseau et plasticité cristalline dans les pyroxènes: une revue. Bull. Mineral., 109: 377–394.

Drury, M.R. and Urai, J.L., 1990. Deformation-related recrystallization processes. Tectonophysics, 172: 235–253.

Ellis, D.J. and Green, D.H., 1979. An experimental study of the effect of Ca upon garnet-clinopyroxene Fe-Mg exchange equilibria. Contrib. Mineral. Petrol., 71: 13–22.

Etheridge, M.A., 1975. Deformation and recrystallization of orthopyroxene from the Giles complex, Central Australia. Tectonophysics, 25: 87–114.

Etheridge, M.A. and Vernon, R.H., 1983. Comment and reply: Seismic velocity and anisotropy in mylonites and the reflectivity of deep crustal fault zones. Geology, 11: 487–488.

Fountain, D.M., Hurich, C.A. and Smithson, S.B., 1984. Seismic reflectivity of mylonitic zones in the crust. Geology, 12: 195–198.

Fountain, D.M., Salisbury, M.H. and Percival, J., 1990. Seismic structure of the continental crust based on rock velocity measurements from the Kapuskasing uplift. J. Geophys. Res., 95(B2): 1167–1186.

Gardner, G.H.F., Wyllie, M.R.J. and Droschak, D.H., 1965. Hysteresis in the velocity–pressure characteristics of rocks. Geophysics, 30: 111–134.

Graham, C.M. and Powell, R., 1984. A garnet-hornblende geothermometer: calibration testing, and application to the Pelona Schist, southern California. J. Metamorph. Geol., 2: 13–21.

Hammarstrom, J.M. and Zen, E-An, 1986. Al in hornblende, an empirical igneous geobarometer. Am. Mineral., 71: 1297–1313.

Handy, M.R. 1990. The solid-state flow of polymineralic rocks. J. Geophys. Res., 95: 8647–8661.

Hanmer, S., Ji, S., Darrach, M. and Kopf, C., 1991. Tantato domain, northern Saskatchewan: a segment of the Snowbird tectonic zone. Current Res., Part C, Geol. Surv. Can., pp. 121–133.

Hanmer, S., Darrach, M. and Kopf, C., 1992. The east Athabasca mylonite zone: an Archean segment of the Snowbird tectonic zone in Northern Saskatchewan. Current Res., Part C, Geol. Surv. Can., pp. 19–29.

Hollister, L.S., Grissom, G.C., Peters, E.K., Stowell, H.H. and Sisson, V.B., 1987. Confirmation of the empirical correlation of Al in hornblende with pressure of solidification of calc-alkaline plutons. Am. Mineral., 72: 231–239.

Hodges, K.V. and Spear, F.S., 1982. Geothermometry, geobarometry and the Al_2SiO_5 triple point at Mt. Moosilauke, New Hampshire. Am. Mineral., 67: 1118–1134.

Jeffery, G.B., 1922. The motion of ellipsoid particles im-

mersed in a viscous fluid. R. Soc. London Proc., A/102: 161–179.

Ji, S. and Mainprice, D., 1988. Natural deformation fabrics of plagioclase: Implications for slip systems and seismic anisotropy. Tectonophysics, 147: 145–163.

Ji, S. and Mainprice, D., 1989. Seismic anisotropy in the lower crust induced by the lattice preferred orientation of minerals. Seismol. Geol. (China), 11(4): 15–30.

Ji, S. and Mainprice, D., 1990. Recrystallization and fabric development in plagioclase. J. Geol., 98: 65–79.

Ji, S. and Salisbury, M., 1993. Shear-wave velocities, anisotropy and splitting in high grade mylonites. Tectonophysics, 221: 453–473.

Ji, S. and Zhao, P., in press. Strength of two-phase rocks: a model based on fiber-loading theory. J. Struct. Geol.

Jones, T. and Nur, A., 1984. The nature of seismic reflections from deep crustal fault zones. J. Geophys. Res., 89: 3153–3171.

Keen, C.E. and Barrett, D.L., 1971. A measurement of seismic anisotropy in the Northeast Pacific. Can. J. Earth Sci., 8: 1056–1064.

Kern, H., 1982. P- and S-wave velocities in crustal and mantle rocks under the simultaneous action of high confining pressure and high temperature and the effect of the rock microstructure. In: W. Schreyer (Editor), High Pressure Research in Geosciences. Schweizerbartsche, Stuttgart, pp. 15–45.

Kern, H. and Schenk, V., 1985. Elastic wave velocities in rocks from a lower crustal section in southern Calabria (Italy). Phys. Earth Planet. Int., 40: 147–160.

Kern, H. and Schenk, V., 1988. A model of velocity structure beneath Calabria, southern Italy, based on laboratory data. Earth Planet. Sci. Lett., 87: 235–337.

Kern, H. and Wenk, H.R., 1990. Fabric-related velocity anisotropy and shear wave splitting in rocks from the Santa Rosa mylonite zone, California. J. Geophys. Res., 95(B7): 11,213–11,223.

Kronenberg, A., 1981. Quartz preferred orientations within a deformed pebble conglomerate from New Hampshire, U.S.A., Tectonophysics, 79: T7–T15.

Kruhl, J.H., 1987. Preferred lattice orientations of plagioclase from amphibolite and greenschist facies rocks near the Insubric line (Western Alps). Tectonophysics, 135: 233–242.

Leven, J.H., Finlayson, D.M., Wright, C., Dooley, J.C. and Kennettand, B.L.N. (Editor), 1990. Seismic probing of continents and their margins, Tectonophysics, special issue, 173, 639 pp.

Mainprice, D., 1990. A FORTRAN program to calculate seismic anisotropy from the lattice preferred orientation of minerals. Comput. Geosci., 16: 385–393.

Mainprice, D. and Nicolas, A., 1989. Development of shape and lattice preferred orientations: applications to the seismic anisotropy of the lower crust. J. Struct. Geol., 11: 175–189.

Mainprice, D., Bouchez, J.L., Blumenfeld, P. and Tubia, J.M., 1986. Dominant c-slip in naturally deformed quartz: implications for dramatic plastic softening at high temperature. Geology, 14: 812–822.

McDonough, D.T. and Fountain, D.M., 1988. Reflection characteristics of a mylonite zone based on compressional velocities of rock samples. Geophys. J., 93: 547–558.

McSkimin, H.J., Anreatch, J.R. and Thurston, R.N., 1965. Elastic moduli of quartz versus hydrostatic pressure at 25° and −195.8°C.J. Appl. Phys., 36: 1624–1632.

Meissner, R., 1973. The Moho as a tranistion zone. Geophys. Surv., 1: 195–216.

Meissner, R., Wever, T. and Sadowiak, P., 1991. Continental collisions and seismic signature. Geophys. J. Int., 105: 15–23.

Mercier, J.-C.C., 1985. Olivine and pyroxene. In: H.R. Wenk (Editor), Preferred Orientation in Deformed Metals and Rocks: An Introduction to Modern Texture Analysis. Academic Press, New York, NY, pp. 407–430.

Moecher, D.P., Essene, E.J. and Anovitz, L.M., 1988. Calculation and application of clinopyroxene-garnet-plagioclase-quartz geobarometers. Contrib. Mineral. Petrol., 100: 92–106.

Montardi, Y. and Mainprice, D., 1987. A TEM study of the natural plastic deformation of calcic plagioclase (An68–70). Bull. Minéral., 110: 1–14.

Nazé, L., Doukhan, N., Doukhan, J.C. and Latrous, K., 1987. A TEM study of lattice defects in naturally and experimentally deformed orthopyroxenes. Bull. Mineral., 110: 497–512.

Newton, R.C. and Haselton, H.T., 1981. Thermodynamics of the garnet-plagioclase-Al_2SiO_5-quartz geobarometer. In: R.C. Newton, A. Navrotsky and B.J. Wood (Editors), Thermodynamics of Minerals and Melts. Adv. Physival Geochemistry, 1: 131–147.

Nicolas, A. and Poirier, J.P., 1976. Crystalline Plasticity and Solid State Flow in Metamorphic Rocks. Wiley, New York, 444 pp.

Olsen, T.S. and Kohlstedt, D.L., 1984. Analysis of dislocations in some naturally deformed plagioclase feldspar. Phys. Chem. Mineral., 11: 153–160.

Perkins, D. III and Newton, R.C., 1981. Charnockite geobarometers based on coexisting garnet-pyroxene-plagioclase-quartz. Nature, 292: 144–146.

Prior, D.J., Knipe, R.J. and Handy, M.R., 1990. Estimates of the rates of microstructural changes in mylonites. In: R.J. Knipe and E.H. Rutter (Editors), Deformation Mechanisms, Rheology and Tectonics. Geol. Soc. Spec. Publ., 54: 309–319.

Raitt, R.W., Shor, G.G., Francis, T.J.G. and Morris, G.B., 1969. Anisotropy of the Pacific upper mantle. J. Geophys. Res., 74: 3095–3109.

Reynard, B., Gillet, P. and Willaime, C., 1989. Deformation mechanisms in naturally deformed glaucophanes: a TEM and HREM study. Eur. J. Mineral., 1: 611–624.

Ribe, N.M., 1989. A continuum theory for lattice preferred orientation. Geophys. J., 97: 199–207.

Ribe, N.M. and Yu, Y., 1991. A theory for plastic deformation and textural evolution of olivine polycrystals. J. Geophys. Res., 96(B5): 8325–8335.

Seront, B., Mainprice, D. and Christensen, N.I., 1989. The complete seismic properties of an anorthosite: comparison between LPO and laboratory measurements. EOS, 70: 460–461.

Schmid, S.M. and Casey, M., 1986. Complete fabric analysis of some commonly observed quartz c-axis patterns. Am. Geophys. Union, Geophys. Monogr., 36: 263–286.

Schwerdtner, W.M., 1964. Preferred orientation of hornblende in a banded gneiss. Am. J. Sci., 262: 1212–1229.

Sheriff, R.E., 1975. Factors affecting seismic amplitudes, Geophys. Prospect., 23: 125–138.

Siegesmund, S. and Kern, H., 1990. Velocity anisotropy and shear-wave splitting in rocks from the mylonite belt along the Insubric Line (Ivrea Zone, Italy). Earth Planet. Sci. Let., 99: 29–47.

Siegesmund, S., Takeshita, T. and Kern, H., 1989. Anisotropy of Vp and Vs in an amphibolite of the deeper crust and its relationship to the mineralogical, microstructural and textural characteristics of the rock. Tectonophysics, 157: 25–38.

Skrotzki, W., 1990. Microstructure in hornblende of a mylonitic amphibolite. In: R.J. Knipe and E.H. Rutter (Editors), Deformation Mechanisms, Rheology and Tectonics. Geol. Soc. Spec. Publ., 54: 321–325.

Starkey, J. and Cutforth, C., 1978. A demonstration of the interdependence of the degree of quartz preferred orientation and the quartz content of deformed rocks. Can. J. Earth Sci., 15: 841–847.

Tullis, J. and Yund, R.A., 1987. Transition from cataclastic flow to dislocation creep of feldspar: mechanisms and microstructures. Geology, 15: 606–609.

Wang, C.Y., Okaya, D.A., Ruppert, C., Davis, G.A., Guo, T.S., Zhong, Z.Q. and Wenk, H.R., 1989. Seismic reflectivity of the Whipple Mountain shear zone, Southern California. J. Geophys. Res., 94: 2989–3005.

Warner, M., 1990. Absolute reflection coefficients from deep seismic reflections. Tectonophysics, 173: 15–23.

Wells, P.R.A., 1977. Pyroxene thermometry in simple and complex systems. Contrib. Mineral. Petrol., 62: 129–139.

Wenk, H.R. and Christie, J.M., 1991. Comments on the interpretation of deformation textures in rocks. J. Struct. Geol., 13(10): 1091–1110.